Proposal to PAC38

Polarized Electrons for Polarized Positrons:
A proof–of–principle experiment

Hari Areti[1], Maud Baylac[2], Germain Bosson[2], Alexandre Camsonne[1], Lawrence Cardman[1], Olivier Dadoun[3], Jonathan Dumas[1,2], Erica Fanchini[2], Tony Forest[5], Arne Freyberger[1], Serkan Golge, Joseph Grames[1], Paul Guèye[4], Yujong Kim[1,5], Jean-François Muraz[2], Marc Marton[2], Matt Poelker[1], Jean-Sébastien Réal[2], Riad Suleiman[1], Alessandro Variola[3], Eric Voutier[2]

[1] *Thomas Jefferson National Accelerator Facility*
12000 Jefferson Avenue
Newport News, Virginia 23606, USA

[2] *Laboratoire de Physique Subatomique et de Cosmologie*
IN2P3/CNRS, Université Joseph Fourier, INP
53 rue des Martyrs
38026 Grenoble cedex, France

[3] *Laboratoire de l'Accélérateur Linéaire*
IN2P3/CNRS, Université Paris-Sud
Bât. 200 - BP 34
91898 Orsay cedex, France

[4] *Physics Department*
Hampton University
Hampton, VA 23668, USA

[5] *Department of Physics and Idaho Accelerater Center*
Idaho State University
Pocatello, ID 83209, USA

Proposal as of 21 June 2011

Contact persons: grames@jlab.org, voutier@lpsc.in2p3.fr

Abstract

We need to generate an abstract for this part of the proposal - no more than 1/3 of a page.

Table of contents

1 Introduction

Polarized and unpolarized positron beams are essential complements to polarized and unpolarized electron beams as tools to further our understanding of nature at distance scales ranging from the frontiers of high energy physics to solid state physics (see ref. [JPos09] for an overview). The PEPPo experiment (Polarized Electrons for Polarized Positrons) proposed here is the first step of a program aiming at the development of a polarized positron source that can provide beams with the intensity and other characteristics needed for the hadronic physics program of the JLab 12 GeV Upgrade. This source would take advantage of the tremendous advances in polarized electron sources that have taken place at Jefferson Lab (JLab) together with polarization transfer in electromagnetic processes. The PEPPo experiment, and the program that would follow from its success, would provide information needed to develop related sources for facilities ranging from a number of proposed high energy physics facilities to the very low energies required for condensed matter studies. This proposal was developed following PAC35's enthusiastic endorsement of LOI-10-010, which noted that *"Any accelerator facility, like JLab, using polarized electrons for its physics program would like an intense beam of polarized positrons. This Letter marks a proof of principle experiment that should become a full proposal."*

The power of polarization observables for the study of the structure of matter has been demonstrated in a broad variety of experiments at SLAC, CERN, DESY, RHIC and JLab. Here at JLab, examples include the proton and neutron form factors, their spin-dependent structure functions, and their excitation spectra. The impact of these experiments has made polarized beams an essential feature of the next generation of accelerators and, in particular, of the 12 GeV Upgrade. A major focus of the science program motivating the 12 GeV Upgrade is the study of nucleon structure through the measurement of the Generalized Parton Distributions (GPDs). Theoretical investigations of the GPDs (as well as the analysis of the first exploratory measurements using presently-available beams) have pointed out the value of access to the charge and spin dependent GPDs. This will require the availability of polarized positron beams to complement the available polarized electron beams. This proposal aims to develop a facility at JLab that will demonstrate the promise of a new approach to the problem and establish a facility capable of mounting experiments relevant to optimizing polarized positron sources for both the 12 GeV Upgrade and a variety of other future uses.

A relatively efficient scheme for positron production, widely used in particle accelerators, relies on the creation of electron-positron pairs from high energy photons, and the subsequent capture and acceleration of the useful fraction of the positrons produced. Traditionally, when polarized positrons were needed, they were obtained by storing the captured positrons in a ring and polarizing them via the Sokolov-Ternov effect [Sok64]. To obtain the higher luminosities needed for a linear collider, two alternate approaches have been investigated. Both take advantage of polarization transfer in electromagnetic interactions.

It is well known [Ols59] that the bremsstrahlung process has sensitivities to

polarization. This property has been widely used to produce linearly polarized photon beams from unpolarized electron beams by selecting off-axis photons and to produce circularly polarized photon beams from linearly polarized electron beams by selecting on-axis photons. These processes are routinely used to obtain a linearly and circularly polarized photon beams at several GeV beam energy for use in Hall B at JLab [Mec03].

The two approaches that have been investigated for the International Linear Collider (ILC) use different techniques to produce the needed circularly polarized photon beams: Compton back-scattering of a laser beam off high energy electrons [Omo06], and synchrotron radiation from very high energy electrons traveling through a helical undulator [Ale08]. The production of polarized positrons from polarized bremsstrahlung was also explored [Bes96,Pot97] for possible use in the ILC, but abandoned because of limited performance.

Our proposed experiment will investigate an alternative scheme based on the polarized bremsstralhung process [Dum09a] that takes advantage of recent advances in high-polarization (85%) and high-current ($\sim$1 mA) electron sources [Gra07]. The basic concept for this source is to use the transfer of the longitudinal polarization of electrons to positrons via polarized bremsstrahlung production followed by polarized pair-creation. This approach has the potential to overcome the limitations of the approaches tried to date, and permit the development of a compact, low energy driver for a polarized positron source [Dum09b]. Such a source would be useful for the JLab 12 GeV program. It may also be useful for a number of other future facilities, such as Super-B and ELIC, and for condensed matter physics.

This new approach has never been investigated experimentally. It is the goal of the proposed experiment to demonstrate the basic process and develop a facility that will support the detailed measurements needed to optimize it. The initial experiment will measure in the 2-5 MeV energy range the energy distribution of the positron yield and polarization obtained from a low energy (6.3 MeV) highly-polarized electron beam .

This document is organized as followed. The next section (and three appendices) summarize the potential uses of polarized positron beams that motivate the proposed experiment. This is followed by sections that review the experimental apparatus we plan to construct and install, and the principles of its operation. Finally, the proposed methodology and beamtime requirements for the initial experiment are described in the last section.

2 Motivation

As discussed above, there are three main motivations for mounting the PEPPo experiment: the nucleon structure studies that would be enabled by a polarized positron beam at JLab; the investigation of a new approach to polarized positron sources that has potential use not only for JLab physics but also for high energy and condensed matter physics; and experimental verification

and understanding of some of the EM processes relevant to the production of polarized electron beams.

In this section we review the main motivations for developing a polarized positron source at JLab: the Deeply Virtual Compton scattering studies of nucleon structure using the Generalized Parton Distribution framework that would be carried out using such a source and the tests of the precision of the one-hard-photon exchange approximation used to analyze and interpret electron scattering that such a source (even without polarization) would enable. The further motivation for a follow-on effort that would explore the associated electro-magnetic processes experimentally (to optimize the development of a source based on this technology) is discussed in Appendix I. Potential measurements of two-photon-exchange effects in electron scattering that would provide a benchmark for theoretical calculations of these processes and experimental determination of their details are outlined in Appendix II. Finally, an example of a potential use of such a source for condensed matter studies is sketched in Appendix III.

2.1 Nucleon structure studies via Deeply Virtual Compton Scattering

In the context of the hadronic physics program worked out at JLab, the comparison between electron and positron scatterings is not only an additionnal source of information but also a mandatory step for the extraction of the physics quantities of interest [JPos09]. Further, the accurate investigation of the partonic structure of nucleons and nuclei needs both polarized electrons and polarized positrons.

Generalized parton distributions

It is only recently that a comprehensive picture of the nucleon's structure has started to develop within the framework of the generalized parton distributions (GPDs) [Mul94,Rad97]. These distributions parametrize the partonic structure of the nucleon in terms of correlations between quarks, anti-quarks and gluons, and therefore contain information about the dynamics of this system. The power of this framework for the problem of nucleon structure is demonstrated by the Mellin moments of the GPDs [Die03], which provide a natural link between microscopic and macroscopic properties of the nucleon.

GPDs are universal non-perturbative objects entering the description of hard scattering processes and correspond to the amplitude for removing a parton carrying some longitudinal momentum fraction and restoring it with a different momentum fraction (Fig. 1). In this process, the nucleon receives a four-momentum transfer whose transverse component is Fourier conjugate of the transverse position of the partons. Consequently, GPDs can be interpreted as a distribution in the transverse plane of partons carrying a certain longitudinal momentum [Bur00,Ral02,Die02,Bel02], providing us with the ability to carry out *"femto-tomography"* of the nucleon.

At leading twists, the partonic structure of the nucleon [Die03,Bel05] is described by four quark-helicity-conserving, chiral-even GPDs ($H^q, \widetilde{H}^q, E^q, \widetilde{E}^q$) and four quark helicity flipping and chiral-odd GPDs ($H_T^q, \widetilde{H}_T^q, E_T^q, \widetilde{E}_T^q$), together with eight similar gluon GPDs. In the forward limit ($t \to 0, \xi \to 0$), the optical theorem links the H GPDs to the usual density, helicity, and tranversity distributions measured in deep inelastic scattering (DIS). However, the E GPDs, which involve a flip of the nucleon spin, do not have any DIS equivalent and then constitute a new piece of information about the nucleon structure. The first Mellin moments relate chiral even GPDs to form factors, as E^q with the Pauli electromagnetic form factor and the second Mellin moments relate GPDs to the nucleon dynamics, particularly the total angular momentum carried by the partons, following Ji's sum rule [Ji97]. Similar relations have been proposed which relate chiral odd GPDs to the transverse spin-flavor dipole moment and the correlation between quark spin and angular momentum in an unpolarized nucleon [Bur05].

Deeply virtual Compton scattering

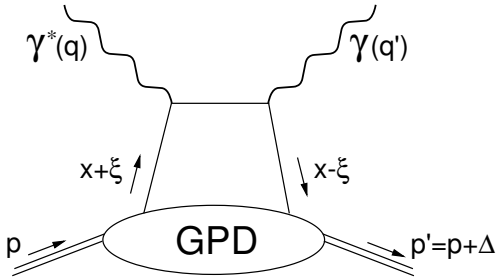

Figure 1. Lowest order (QCD) amplitude for the virtual Compton process.

GPDs can be accessed in the Bjorken regime [Ji98,Col99] of deep exclusive processes, that is when the resolution power of the probe is large enough to resolve partons and when the momentum transfer to the nucleon is small enough to insure the separation of perturbative and non-perturbative scales. Pioneer measurements at HERMES [Air01] and CLAS [Ste01], and recent JLab experiments [Mun06,Maz07,Gir08] have established the relevance of the DVCS process for these studies.

DVCS, corresponding to the absorption of a virtual photon by a quark followed quasi-instantaneously by the emission of a real photon, is the simplest reaction to access GPDs. In the Bjorken regime, the leading contribution to the reaction amplitude is represented by the so-called handbag diagram (Fig. 1), which represents the convolution of a known $\gamma^* q \to \gamma q$ hard scattering kernel with an unknown soft matrix element describing the partonic structure of the nucleon parametrized by GPDs. Consequently, GPDs (E^f) enter the reaction cross section through a Compton form factor $\mathcal{E}$ which involves an integral over the intermediate quark propagator

$$\mathcal{E} = \sum_f e_f^2 \, \mathcal{P} \int_{-1}^{+1} dx \, \left(\frac{1}{\xi - x} - \frac{1}{\xi + x} \right) E^f(Q^2, x, \xi, t) \qquad (1)$$
$$+ i\pi \sum_f e_f^2 \left[E^f(Q^2, \xi, \xi, t) - E^f(Q^2, -\xi, \xi, t) \right] ,$$

leading to a complex DVCS amplitude in which the real and imaginary parts are the quantities of interest to be extracted from experimental data.

In addition to the DVCS amplitude, the cross section for electroproduction of photons has contributions from the Bethe-Heitler (BH) process where the real photon is emitted by the initial or final lepton, leading to [Die09]

$$\sigma(ep \to ep\gamma) = \sigma_{BH} + \sigma_{DVCS} + P_l \, \widetilde{\sigma}_{DVCS} + e_l \, \sigma_{INT} + P_l e_l \, \widetilde{\sigma}_{INT} \qquad (2)$$
$$+ S \left[P_l \, \Delta\sigma_{BH} + P_l \, \Delta\sigma_{DVCS} + \Delta\widetilde{\sigma}_{DVCS} + P_l e_l \, \Delta\sigma_{INT} + e_l \, \Delta\widetilde{\sigma}_{INT} \right]$$

where the $[\Delta]\sigma(\widetilde{\sigma})$'s are even(odd) function of the out-of-plane angle between the leptonic and hadronic planes; S is the longitudinal or transverse polarization of the target; and P_l and e_l are the lepton polarization and charge, respectively. Though indistinguishable from DVCS, the BH cross section is known and exactly calculable from the electromagnetic form factors. The pure DVCS and interference contributions contain the information of interest, particularly $[\Delta]\sigma_{INT}(\widetilde{\sigma}_{INT})$ is proportionnal to the real(imaginary) part of the DVCS amplitude. The knowledge of the full set of the eight unknown amplitudes participating to the reaction cross section is required in order to separate in a model independent way the different GPDs [Gui08,Mou09]. Considering for simplicity the case of an unpolarized target, the observables measured with a (un)polarized electron beam are

$$\sigma^0(e^-) = \sigma_{BH} + \sigma_{DVCS} - \sigma_{INT} \qquad (3)$$
$$\sigma^+(e^-) - \sigma^-(e^-) = 2P_l \, \widetilde{\sigma}_{DVCS} - 2P_l \, \widetilde{\sigma}_{INT} \qquad (4)$$

where the upper index denotes the polarization state of the beam. Separating further the DVCS and INT contributions requires additionnal measurements at different beam energies within a Rosenbluth like procedure [Ber06] which is known to be limited in the case of elastic electron scattering. The availability of a polarized positron beam allows the measurement of the additional observables

$$\sigma^0(e^+) - \sigma^0(e^-) = 2 \, \sigma_{INT} \qquad (5)$$
$$\left[\sigma^+(e^+) - \sigma^+(e^-) \right] - \left[\sigma^-(e^+) - \sigma^-(e^-) \right] = 4P_l \, \widetilde{\sigma}_{INT} \qquad (6)$$

which correspond to a unique determination of the real and imaginary parts of the interference amplitude, free from any additional contributions.

In conclusion, the determination of the eight unknown contributions to the cross section for electroproduction of photons and the subsequent extraction

of the nucleon GPDs require the measurement of eight independent observables that can be uniquely determined by combining polarized electron and polarized positron data.

2.2 Studies of the precision of the one hard photon exchange approximation in elastic electron scattering

A second motivation for the development of a positron source at JLab is the capability of improving tests of the precision of the one hard photon exchange approximation in elastic electron scattering. The nucleon electromagnetic form factors are fundamental quantities that relate to the charge and magnetization distributions in the nucleon [Kel02,Mil03,Mil07,Arr07,Per07]. Thus, they are important quantities when examining the spatial distribution and dynamics of quarks in the nucleon [Mil03,Mil07,Mil08,Mil09]. The scattering of charged leptons, both electrons and positrons, has long proved to be a powerful tool in nuclear and particle physics. Leptons are pointlike objects that interact with the target via the electromagnetic force and through the exchange of photons. The pointlike probe and the well-understood force mean that the structure of the target can be deduced from the measured differential scattering cross-section. In turn, details of the structure of atoms, nuclei and nucleons have been revealed as the resolving power of the probe improved by increasing the lepton energy. While unpolarized elastic scattering has been used since the 1950s to obtain the proton electric and magnetic form factors, G_E and G_M, using the Rosenbluth separation technique [Ros50], inclusive quasi-elastic scattering on nuclear targets had a strong impact on our knowledge of the single-particle and many particle nuclear properties such as the dynamical measurement of the nuclear Fermi momentum [Whi74], information on high momentum components in nuclear wave function [Ben95], and modification of the nucleon form factor in the nuclear medium [Jou96]. These experiments have been analyzed assuming that a single hard photon is exchanged between the electron and the target during the scattering process.

Recent high Q^2 (virtual photon 4-momentum transfer squared) elastic scattering measurements at Jefferson Lab [Jon00,Gay02,Puc11] showed a striking disagreement with previous measurements [Arr03], as well as a new, high precision extraction using a modified Rosenbluth separation technique [Qat05]. This discrepancy is believed [Gue98,Gui03,Car07] to originate from the contribution of the two-photon exchange (TPE) mechanism that has been neglected. Similarly, quasi-elastic data on nuclear targets have indicated an effect due to the nuclear Coulomb potential that changes the response function because of the repulsion (attraction) of the positive (negative) incident lepton probe [Gue99]. These effects appear to dramatically affect previously reported experimental observations such as the EMC effect [Sol09]. More recently, there is a 5-sigma discrepancy between measurements of the proton charge radius using the Lamb shift in muonic hydrogen [Pho10], and that extracted from electron scattering [Sic03] or the lamb shift of atomic hydrogen [Moh08]. Calculations of Coulomb distortion yield a 1% shift in the proton radius as extracted from electron scattering [Ros00], but these corrections have never been tested against measurements sensitive to the TPE corrections.

The best way to isolate and quantify these corrections is the comparison of electron and positron scattering. Existing data for elastic scattering from the proton has provided only limited evidence for these corrections [Arr04], which have significant impact at both low- and high-energy scattering. Additional experimental tests were carried out recently at JLab [Arr06,Mez11], and improved accuracy is anticipated (the data are in early stages of analysis). Further tests are planned for DESY [OLY08]. However, in both cases the luminosity is still limited relative to what is needed to match the potential accuracy of the electron scattering data. If the approach to positron production planned for PEPPo can be demonstrated to yield a 100 nA beam, it would permit an order of magnitude improvement in the statistical accuracy of e^+/e^- comparisons. In addition, the availability of polarized positron beams would permit the experimental study of the details of the two-photon contributions (see Appendix III).

3 PEPPo apparatus

3.1 Principle of the PEPPo experiment

In this experiment a modest energy (less than 10 MeV) beam of highly spin polarized electrons will strike a conventional pair production target foil. The incident polarized electrons will transfer their polarization via bremmstrahlung and pair production within the target foil. The resulting positrons will be collected and analzyed. The goal of the experiment is to measure the yield and polarization of the resultant positrons as a function of their momenta and the indicent electron beam conditions.

This chapter first introduces CEBAF injector and existing equipment to control and characterize the electron beam and second the new configuration and experimental apparatus of the injector dedicated to the PEPPo experiment.

3.2 Existing Apparatus

The CEBAF polarized electron photoinjector provides the drive beam for the polarized positron experiment. To perform the experiment an electron beam with energy not more than 10 MeV and high polarization is sufficient. In addition, the low energy avoids neutron production and the low current needed (1-10 μA) requires only a low power target. This section describes the critical components to produce and control the polarized electron beam, acceleration and measurement of MeV beam energy, and control of the polarization orientation and its measurements using a Mott electron polarimeter.

3.2.1 Polarized Electron Source

The production of the polarized beam results from the excitation of a Gallium Arsenide (GaAs) semiconductor with circularly polarized laser photons. The polarization of the electrons comes from the optical pumping between the $P_{3/2}$ valence band and the $S_{1/2}$ conduction band levels. The spin of atomic electrons $m_s = \pm 1/2$ and the orbital angular momentum m_l (the orbital l corresponds to $2l + 1$ values of m_l, hence $m_l = -1, 0, 1$ for the P valence band and $m_l = 0$ for the S conduction band) make a spin substate degeneracy with characteristic total angular momentum $m_j = m_l + m_s$ (two degenerated spin substates with $m_j = \pm 1/2$ are then possible for S and four for P with $m_j = -3/2, -1/2, 1/2, 3/2$). The minimum energy gap between $P_{3/2}$ and $S_{1/2}$ energy levels is 1.43eV corresponding to the laser photon energy required for electron extraction. Right(Left)-circularly laser photons lead then to preferential $\Delta m_j = 1$ ($\Delta m_j = -1$) transitions between the valence and conduction bands. Besides, the electron excitation from $m_j = -3/2$ ($m_j = 3/2$) of the valence band to the $m_j = -1/2$ ($m_j = 1/2$) of the conduction band is three times more likely to occur than from $m_j = -1/2$ ($m_j = 1/2$) of the valence band to the $m_j = -1/2$ ($m_j = 1/2$) of the conduction band as indicated by the Clebsh-Gordon coefficient[?] indicated on Fig. 2.

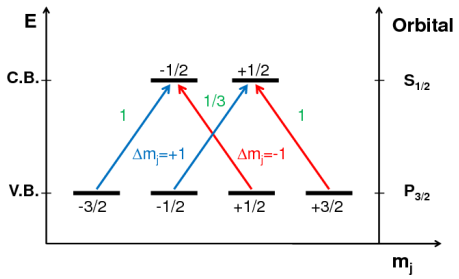

Figure 2. The transition of the atomic electron bound state in GaAs for a right(left)- circularly polarized laser photon are represented by the blue(red) arrows. Relative amplitudes of preferential transitions are in green.

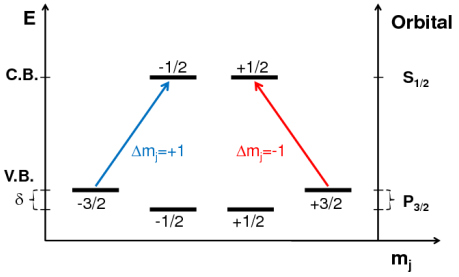

Figure 3. The transition of the atomic electron bound state in the activated GaAs/GaAsP for a right(left)-circularly polarized laser photon are represented by the blue(red) arrows. δ is the energy gap breaking the degenerated spin substates of $P_{3/2}$.

This results in a theoretical limit of 50% polarized electrons. The polarization can be increased by shifting the $m_j = \pm 3/2$ above the $m_j = \pm 1/2$ substate energy levels. This degeneracy in GaAs may be removed by providing a strain to the crystal structure. A suitable strain at the atomic level is accomplished by growing altnernating layers a few nanometers thick of GaAs and GaAsP (phosphorous dopant). The resultant difference in GaAs lattice spacing provide a suitable strain that lifts the degeneracy. The difference between $m_j = -1/2$ and $m_j = -3/2$ of $P_{3/2}$ is of the order of δ=0.1 eV, to eliminate the the limitation of 50% (Fig. 3). In reality depolarization of the electrons occur as they scatter during the photoemission process. So-called superlattice strained GaAs photocathode provide polarization as high as 90%.

Spin polarized photoemission ultimately depends upon the capability for electrons reaching the conduction band to leave the crystal. Generally, the electronic affinity of GaAs, E_a, prevents the conduction band electrons from leaving the crystal and pass to the vacuum, see Fig. 4. The electronic affinity is about 4eV for GaAs but may be reduced to zero if a layer of alkali such as Cesium (Cs) is applied at the GaAs surface. The oxidation of that layer with nitrogen trifluoride (NF_3) further reduce the electron affinity to become negative, allowing electrons reaching the conduction band to tunnel through the surface barrier potential and exit the crystal into the vacuum.

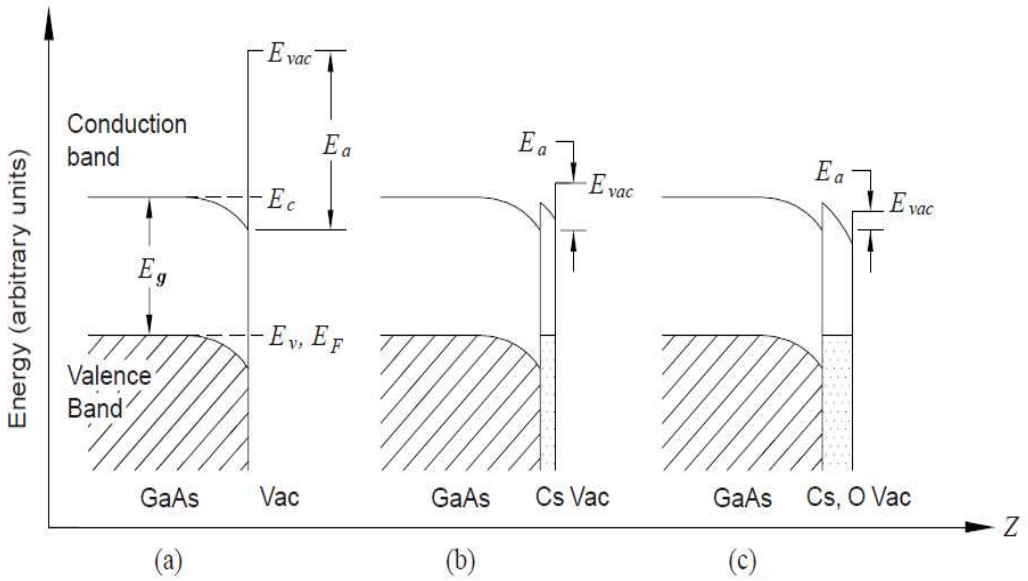

Figure 4. GaAs electronic affinity and band structure at the surface of the crystal; (a) Bulk GaAs; (b) GaAs with a layer of Cesium; (c) GaAs with a layer of Cesium and oxydant NF_3

Quantitatively, the number of electrons extracted $q_{extracted}$ from the GaAs photocathode per laser photon N_γ is termed the quantum efficiency (QE),

$$QE = \frac{q_{extracted}}{N_\gamma}. \tag{7}$$

or in terms of incident laser power P_{gamma} and photon energy $h\nu$ as

$$I_e = QE\frac{P_\gamma}{h\nu}. \tag{8}$$

The photocathode is illuminated by a fiber-based laser which consists of three stage components; firt, a gain-switched fiber-couple 1560 nm diode seed laser syncrhonized to the accelerating cavity radio-frquency signal, followed by a ErYb-doped fiber amplifier to increase the power at 1560 nm and ultimately a periodically poled lithium niobate (PPLN) frequency doubler which results in 780 nm suitable to optically pump the spin polarized state of the superlattice GaAs/GaAsP photocathode. Optical pulses with duration of about 40 ps

are directed by mirrors and through polarization controlling optics through a vacuum beam line window and focused to about 0.5 mm spot of the photocathode. The linearly polarized laser light is converted to either left/right circular polarization by an electro-optic Pockels cell which can set the laser (and electron) helicity at nearly 1 kHz. In additional, optical quarter-wave plate may be inserted/retracted to change the overall sign of the laser helicity.

The photocathode itself is fixed in the cathode electrode of the high voltage photogun at a short distance in front of a grounded anode electrode. Circularly polarized laser light illuminating an activated photocathode will photoemit electrons which are accelerated across the cathode/anode electrode gap thus attaining the energy of the high voltage power supply. These semi-relativistic electrons emitted synchronously with the accelerator radio-frequency have an initial bunch length comparable to the optical pulse length, are 130 kV (semi-relativisitc) and form the basis for the electron beam.

3.2.2 Electron Beam Energy and Measurement

The beam energy is defined by a sequence of electron acceleration. Electrons emitted from the photocathode are accelerated across a potential gap of 130 kV sustained by an external high voltage power supply. All subsequent acceleration is by radio-frequency cavities with a fundamental frequency of 1497 MHz, the same as the time structure produced at the source. The first cavity is a room temperature 5-cell graded-beta cavity constructed from copper which accelerates the electrons to 500 keV. Acceleration to higher energy is accomplished using two 5-cell niobium cavities. Power is distributed from high power klystrons in a ground level service building, into the accelerator enclosure via an RF waveguide under vacuum and through a ceramic vacuum window to the cavity itself. The cavities are directly part of the accelerator beam line through which the electron beam passes. The power to each cavity is controlled by a gradient setpoint and monitored by a gradient readback. These cavities are submersed in a bath of liquid helicum and become superconducting which allow for continuous operation compatible with the 100% duty factor electron beam. The maximum stable cavity gradients achieved were 8.4 MV/m and 6.1 MV/m. Each cavity has an effective length of 0.5m indicating a total energy of 7.25 MeV is achievable by the cryounit. In summary, the total electron beam can attain a maximum beam energy of about 7.75 MeV. To precisely know the beam energy a momentum spectrometer is used. The relation between momentum, magnetic field and deflected angle is given by:

$$\frac{pc}{e} = \frac{\int Bdl}{\theta}, \tag{9}$$

where e is the electronic charge (1.602×10^{-19} C), c is the speed of light (2.99×10^{8}m/s), θ is the deflection angle in radians and $\int Bdl$ is the integrated magnetic field along the deflected orbit. Experimentally the bend angle is determined by beam position monitorss which measure the indicent beam direction and scanning wire diagnostic which defines the deflected beam direction through a dipole magnet of known magnetic profile.

The precision of the beam momentum is determined by - Jon, you fill in this information.

3.2.3 4π Spin Rotators and Mott Electron Polarimeter

Control and knowledge of the electron beam polarization is cruical to calibration and interpretation of the positron polarimetry. The electron beam is polarized parallel or anti-parallel to the beam momentum of electrons emitted at the photocathode defined by

$$\mathrm{P} = \frac{N_\uparrow - N_\downarrow}{N_\uparrow + N_\downarrow} \tag{10}$$

where $N_\uparrow (N_\downarrow$ is the number of electrons with a spin $\frac{\hbar}{2}(-\frac{\hbar}{2})$ is aligned with the beam direction.

The overall sign (helicity) of the photoemitted electrons are fundamentally controlled by defined the sign of the circular laser polarization. Typical methods to do this (Pockels cell, wave plate retarders) are described in the earlier section. Once the electron beam is formed the mean value of the electron polarization is conserved however the orientation in space may be transformed by rotations using electro-magnetic fields of either Wien filters or solenoids.

Wien filters present crossed electric and magnetic fields which do no alter the electron beam trajectory but rotate the the polarization about an axis transverse to the beam momentum (see Fig. 5). The magnetic field rotates the beam and its polarization by an angle ϕ_{spin} as

$$\phi_{spin} = \frac{(g-2)}{2m_e}.E_{beam}.\theta_{bend} \tag{11}$$

where g is the electron gyromagnetic factor and $\theta_{bend} = p/e.\int B.dl$ is the bending angle of the beam in the magnetic field. The polarization can be rotate independently from the beam direction as a perpendicular electric field E evens out the Lorentz force:

$$\vec{F} = q\Big(\vec{E} + \frac{\vec{\beta}}{c} \wedge \vec{B}\Big) = 0 \tag{12}$$

The Wien filter requires that $E = \beta B$

Solenoids present a longitudinal magnetic field which similarly does not deflect the electron beam trajectory but rotate the polarization about the axis of the beam moementum.

Jon, you should similarly add text here showing or describing rotation of spin in a solenoid.

By sequencing a vertical Wien filter, followed by Solenoids, followed by a horizontal Wien filter the three successive rotations about the X, Z and Y axis may set the polarization to any orientation in 4π.

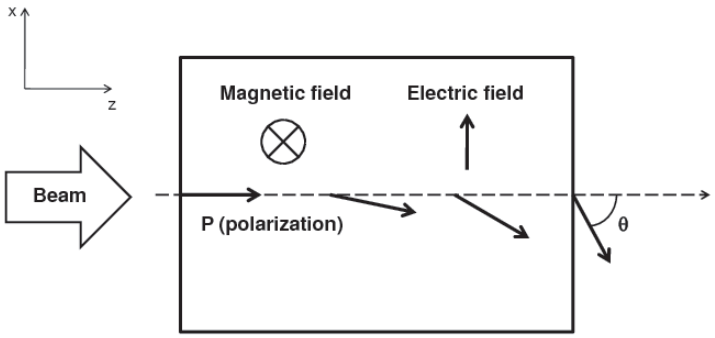

Figure 5. Wien filter in which an electric $\vec{E}$ and magnetic $\vec{B}$ field are applied to rotate the particles spin with an angle θ and preserving their momentum.

3.2.4 Mott Electron Polarimeter

A Mott electron polarimeter exits on a dedicated beam line following the cryounit which may be used to measure orthogonal components of the electron polarization normal to the beam direction (beam momentum). The polarimeter relies on the interaction of the electron spin with the nuclear potential of an unpolarized target.

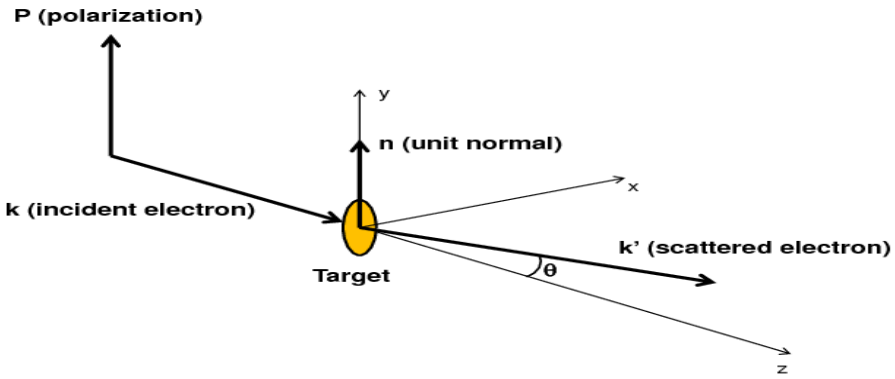

Figure 6. Mott scattering for a transversely polarized beam.

The magnetic field provided by the electron motion in the nucleus electric field and the electron magnetic moment (related to the spin) results in a spin-orbit coupling in the electron scattering potential and leads to a spin dependent

component in the Mott cross section

$$\frac{d\sigma}{d\theta} = \frac{\sigma_0}{d\theta}\left[1 + S(\theta)\vec{P}.\hat{n}\right] \tag{13}$$

where the unpolarized cross section component is

$$\frac{d\sigma_0}{d\theta} = \left(\frac{Ze^2}{2mc^2}\right)^2 . \frac{(1-\beta^2)(1-\beta^2\sin^2(\theta/2))}{\beta^4 \sin^4(\theta/2)} \tag{14}$$

$\vec{n}$ is the unitary vector normal to a plane defined by the incident and scattered electron as

$$\hat{n} = \frac{\vec{k} \times \vec{k'}}{|\vec{k} \times \vec{k'}|} \tag{15}$$

E is the electron beam energy, r_0 is the electron radius, e is the Coulomb charge and $S(\theta)$ is the Sherman function. The electron polarization $\vec{P}$ component transverse to the scattering plane (colinear with $\hat{n}$) generates a contribution to the polarized Mott cross section. The asymmetry ϵ of electron scattering at two (symmetric) angles ($\pm\theta$) with the electron beam direction is given by

$$\mathrm{P} = \frac{N_{+\theta} - N_{-\theta}}{N_{+\theta} + N_{-\theta}} = P_{beam} S(\theta) \tag{16}$$

The Sherman function determines the experimental asymmetry or analyzing power of the polarimeter and can be maximized with a) the atomic number Z (spin-coupling increases with large Z) of the target (Fig. 7), b) the electron beam energy (Fig. 8) and c) the scattering angle θ. For a 5 MeV electron beam, the Sherman function is maximized at a scattering angle of $\pm 173^\circ$. Thin gold targets (ranging from 0.1 μm to 5 μm) are used to minimize multiple scattering. The polarimeter measures a transverse polarization, so in order to measure the longitudinal component of the beam polarization, the electron spin needs to be redirected with a Wien filter.

3.3 PEPPo Experimental Apparatus

The PEPPo experimental apparatus planned for this experiment is comprised of 5 successive beam line regions. Regions 0 describes the transition from the CEBAF injector to Regino 1, a new dedicated beam line for with the purpose to control and measure the electron beam parameters up to the conversion target. Region 2 is comprised of a solenoid magnet to spatially collect positrions and a spectrometer with an energy collimator to further refine the desired momenta. Region 3 is a short diagnostic line to quantify the positron yield and distribution. Finally, Region 4 is a Compton transmission polarimeter. It is noteworthy that by choosing the polarity of magnets in Regions 2-4 either one may either transport the incident electron beam (target out) or choose to collect either positrons or electrons (target in).

The five regions are shown here: positron production, the collection of positrons and finally the polarimetry, see Fig. 9

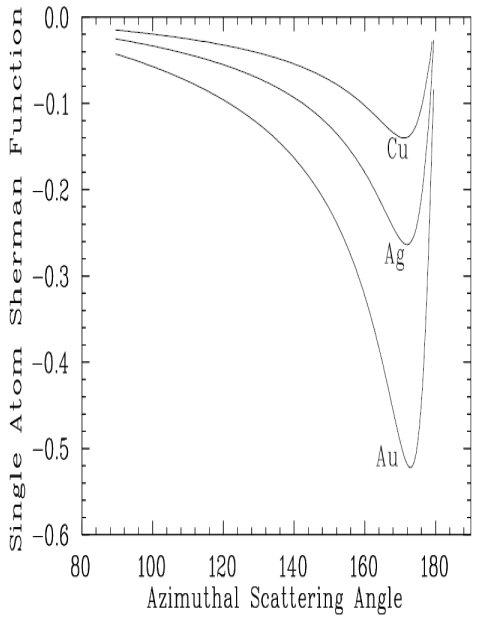

Figure 7. Sherman function for different materials: copper (Z=29), silver (Z=47) and gold (Z=79).

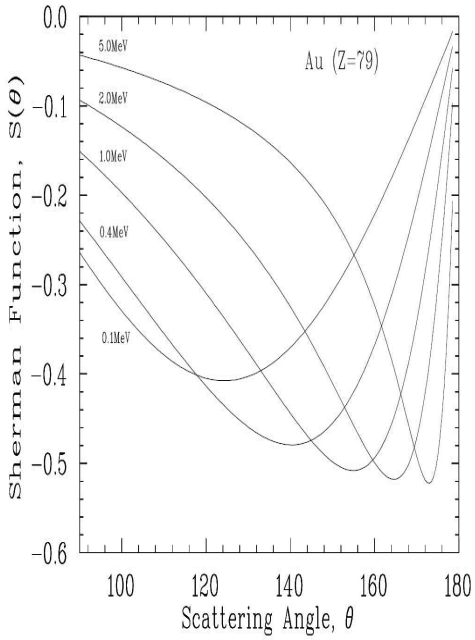

Figure 8. Sherman function for different beam energies.

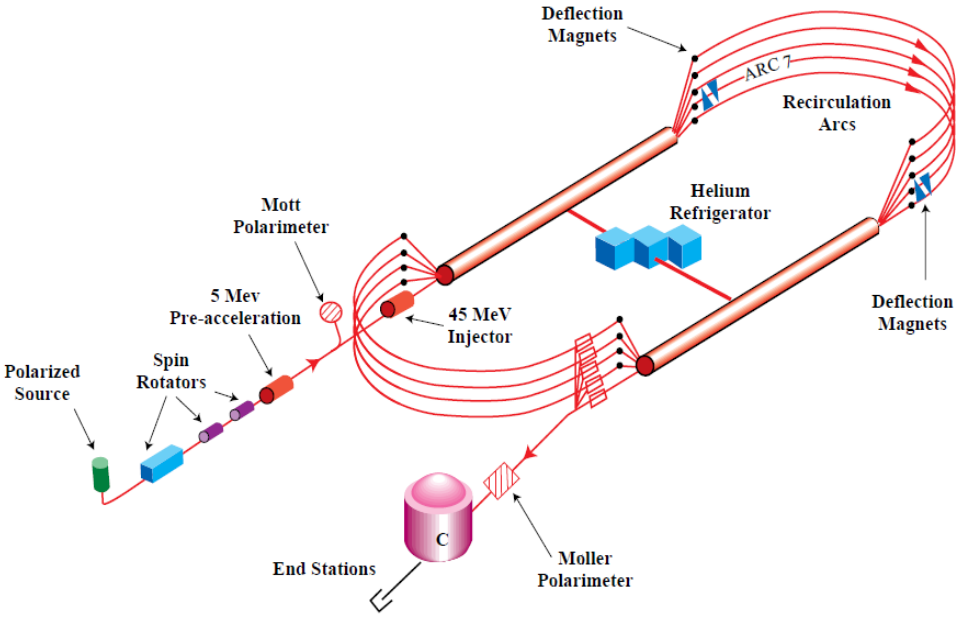

Figure 9. *positron segment added to the existing injector beamline*

3.3.1 Region 0 - CEBAF Injector

The Region 0 of the PEPPo experiments is a part of an existing CEBAF injector beamline between a viewer (ITV0L01) and a dipole (MBV0L021) as shown in Fig. 10. By tuning strength of existing three quadrupoles (MQJ0L01,

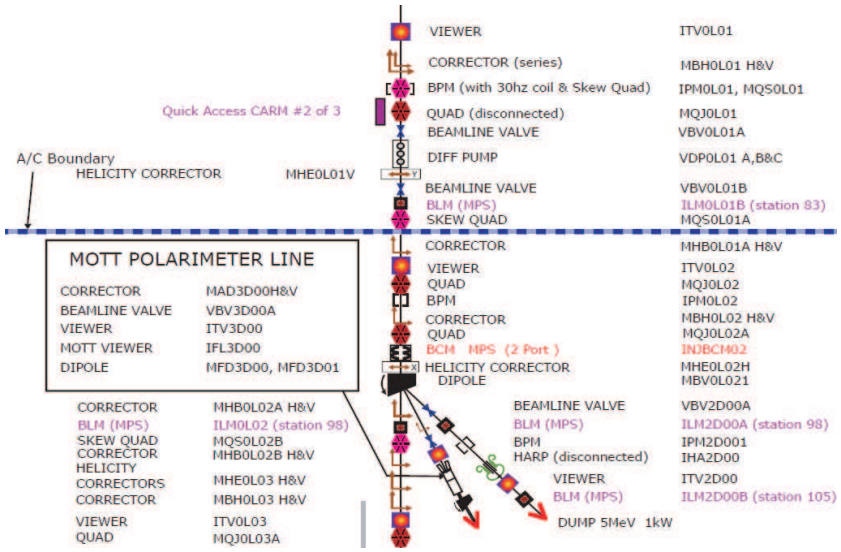

Figure 10. Layout of the Region 0 of the PEPPo beamline.

MQJ0L02, and MQJ0L02A) in the Region 0, we can adjust the transverse beam size or beam diameter at the electron-positron converting target, which is the first target at the Region 1. To match the electron beam optics along the PEPPo beamline, the transverse electron beam emittance and twiss parameters (α, β, γ) will be measured by using a well-known quadrupole scanning method. To perform the quadrupole scanning method, a quadrupole (MQJ0L01) and the second viewer (ITV0L02) in the Region 0 will be used. Electron beam energy and energy spread will also be measured with the dipole magnet and a viewer (ITV2D00) in the -30 deg spectrometer beamline as shown in Fig. 10. These measured twiss parameters, transverse beam emittance, energy, and energy spread will be used to update a design optics of electron beams along the PEPPo beamline. For the PEPPo experiments, a new branching beamline (+25 degree beamline) will be added to the dipole, and the dipole will be rotated to make the pole face angles of the dipole magnet perpendicular to the beam trajectory of the 0 degree CEBAF injector beamline shown in Fig 11. Since the maximum value of multiplication of the magnetic field and the effective length of the dipole magnet is about 14833 G-cm for a maximum power supply current of 3.5 A, its maximum bending angle is about 33.8 degrees for an 8 MeV electron beam. Therefore, by adjusting the current of the magnet power supply, the dipole can supply electron beams to four branching beamlines (-30 degree spectrometer, -12.5 degree Mott polarimeter, 0 degree CEBAF injector, and +25 degree PEPPo) freely as shown in Figs. 11 and 12.

3.3.2 Region 1 - PEPPo Electron Beamline

The Region 1 of the PEPPo experiments is a new electron beamline from the MBV0L021 dipole to the electron-positron converting first target, which is located at S = 62.96 in as shown in Fig. 11. Since the natural horizontal dispersion at the first target is about 0.7 m, and the expected relative rms energy spread of the electron beam is about 0.1%, the horizontal beam size is

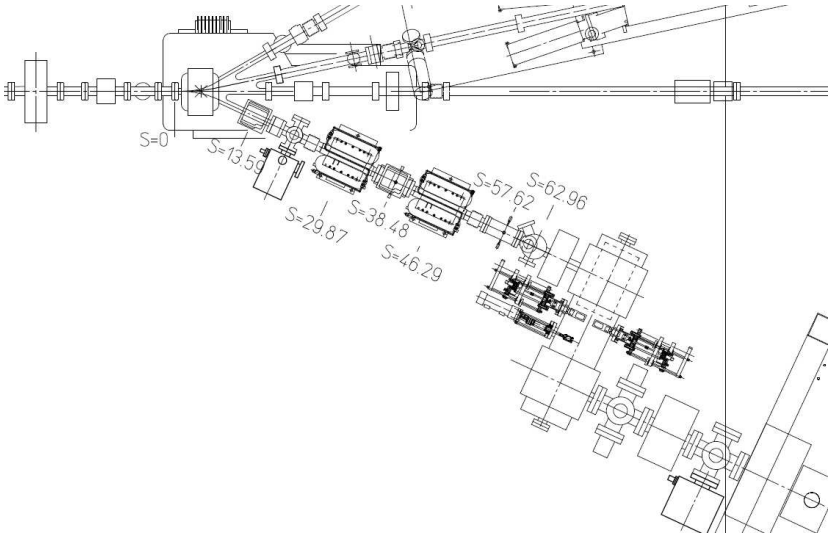

Figure 11. Layout of the Region 1 of the PEPPo beamline. Here the beamline is rotated by -90 degree from the layout in Fig. 10.

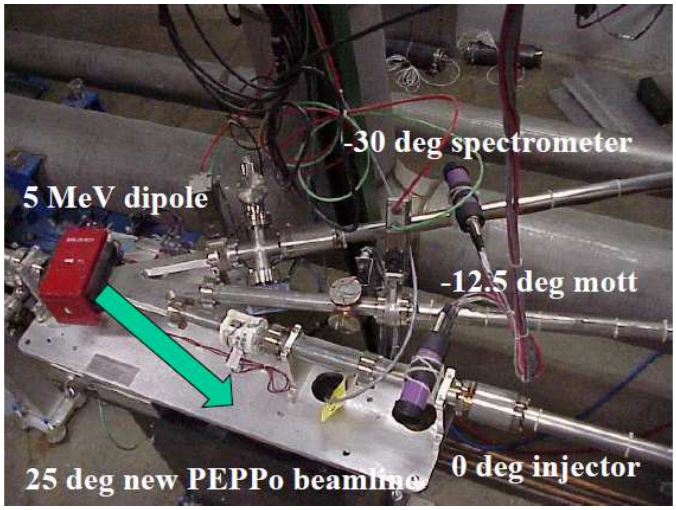

Figure 12. Three existing beamlines and a new PEPPo beamline of a dipole (MBV0L021).

much larger than the vertical beam size if the horizontal dispersion function is not reduced properly. To reduce the horizontal dispersion function at the first target, two new quadrupoles will be installed at S = 29.87 in and S = 46.29 in as shown in Fig. 11. By optimizing the two new quadrupoles in the Region 1 beamline we can reduce the horizontal dispersion function and also make a round beam shape at the first target, as shown in Figs. 13 and 14.

By optimizing the three quadrupoles in the Region 0 beamline and the two quadrupoles in the Region 1 beamline together, the beam diameter at the first target can be adjusted from 1.0 mm to 6 mm, as shown in Fig. 14.

To detect the electron beam's positions and to correct both the positions and the angle of the beam trajectory in the Region 1 beamline, there are two beam

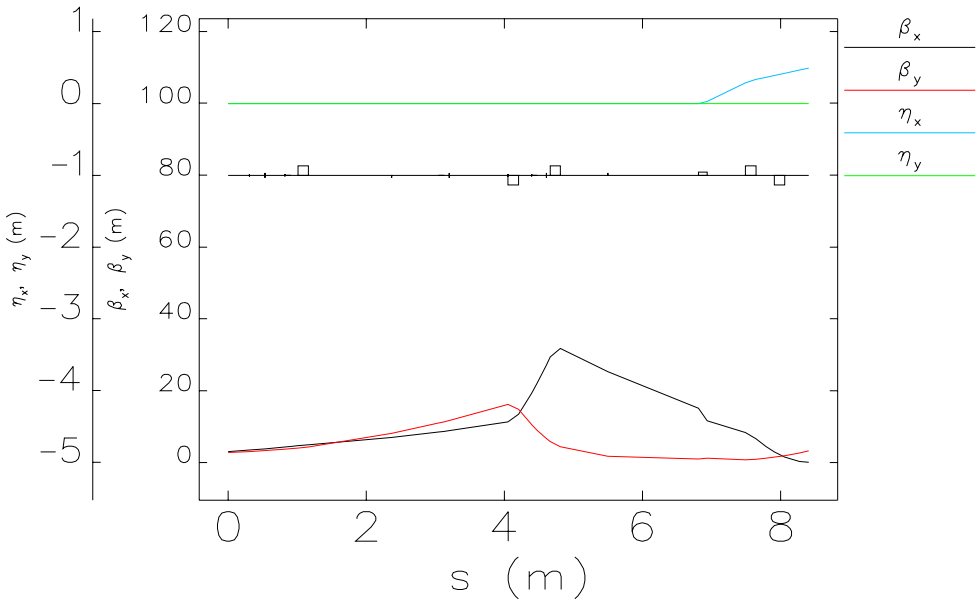

Figure 13. Electron beam optics along the PEPPo Region 0 and 1 to obtain a beam diameter of 3 mm at the first target. Here the beamline starts from 0.3 m upstream from the first viewer (ITV0L01) in the Region 0, and three quadrupoles in Region 0 are located at s $\simeq$ 1.2 m, 4.2 m, and 4.8 m. The MBV0L021 dipole is located at s $\simeq$ 6.9 m, and two new quadrupoles are located at s $\simeq$ 7.6 m and 8.1 m. The first target is located at the end of the beamline, s $\simeq$ 8.4 m.

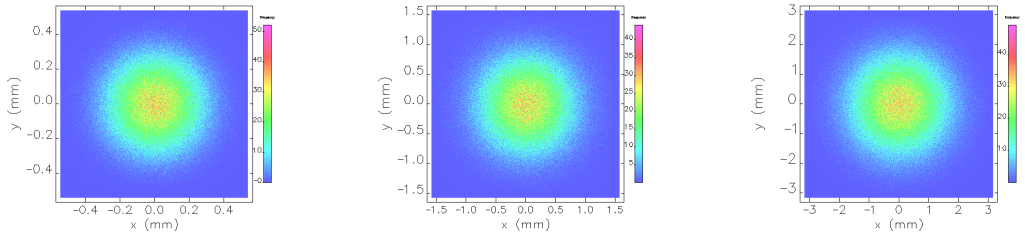

Figure 14. Transverse electron beam profiles at the first target for a beam diameter of 1 mm (left), 3 mm (center), and 6 mm (right).

position monitors (at S = 38.48 in and S = 57.62 in) and two horizontal and vertical steering magnet sets (at S = 13.59 in and S = 38.48 in), as shown in Fig. 11. In addition to the beam position monitors, there are two viewers to measure the beam's energy, energy spread, size, and trajectory, and to measure the horizontal dispersion function in the Region 1 beamline. For a kinetic energy of 6.3 MeV, electron beam parameters and machine parameters are summarized in Table 1.

3.3.3 Region 2 - Target, Capture Solenoid and Spectrometer

*** I think we should use text from Jonathan's thesis ***

Table 1
Beam and machine parameters in the Region 0 and Region 1.

Parameter	Unit	Value
electron kinetic energy	MeV	6.3
relative rms energy spread	%	0.1
rms bunch length	mm	0.3
single bunch charge	fC	20
average electron beam current	μA	10
electron beam operational frequency	MHz	499
initial horizontal alpha-function $\alpha_{x,0}$	·	-0.566
initial vertical alpha-function $\alpha_{y,0}$	·	-0.397
initial horizontal beta-function $\beta_{x,0}$	m	3.076
initial vertical beta-function $\beta_{y,0}$	m	2.798
maximum gradient of quadrupoles	T/m	10
mechanical length of quadrupole	m	0.15
final horizontal beta-function β_x	m	0.098
final vertical beta-function β_y	m	3.299
final horizontal dispersion η_x	m	0.492
rms beam size at the first target	mm	0.5
diameter of electron beam at the 1st target	mm	3
shape of transverse beam profile	·	Gaussian
shape of longitudinal beam profile	·	Gaussian

3.3.4 Region 3 - Diagnostic Line

The Region 3 section of PEPPo is diagnostic, includes annihilation counter and Faraday cup for yield measurements and a fiber array detector for spatial distribution measurements.

Annihilation Counter

*** Tony/Arne add text ***

Scintillating Fiber Array

Because of the very low expected positron current (few 10s-100s pA), special attention was made to evaluate the positron beam profile. For that specific purpose, we will borrow the scintillating fiber array detector used in the two-photon exchange (TPE) experiment that was recently performed in Hall B [Mot09,HallB07] as one of the beamline diagnostic tools for PEPPo. This detector was built as an x-horizontal/y-vertical array to obtain a two-dimensional beam profile. A schematic of this device that was originally designed, built and tested at Florida International University especially for this TPE experiment is shown on Fig. 15. It consists of a 15.24 cm $\times$ 15.24 cm aluminum frame with a 2.54 cm frame width. This frame supports 32 (16 in each direction) thin scintillating fibers each with a 1×1 mm^2 cross section area and a 0.5 mm spacing between each fiber. These fibers are made of a polystyrene core material surrounded by a polymethylmetacrylate (PMMA)

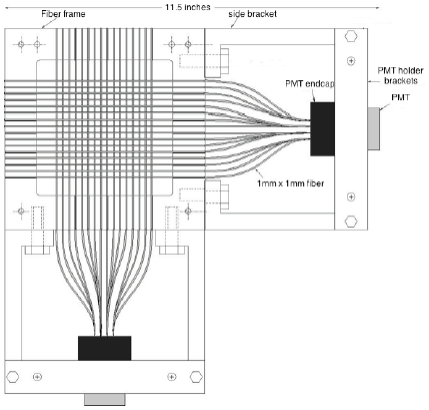

Figure 15. The 32 channel scintillating fiber monitor used in the two-photon exchange experiment in Hall B [HallB07]

layer, multiclad (to optimize internal reflection), of type BCF-12 and have a 42 cm radiation length. They were purchased from Saint-Gobin [Sai11]. Each set of 16 fibers is glued to a 16-channel (4×4 matrix) multianode Hamamatsu H8711 photomultiplier tube.

This device will be located in front of the analyzer magnet described in section 3 and mounted on a 20.32 cm long actuator to allow for a remotely controlled insertion. For the PEPPo experiment, the signal from each fiber will be stored in the data stream as EPICS events and correlated with the other beam diagnostic tools (BeO viewers, beam position monitors and annihilation counter) to understand the optics of the system during the calibration runs and to correct for possible beam offsets during data taking. Being an invasive instrument, we do not intend to use it during actual data taking. Rather, the device will be inserted within the beam in a two-step approach. First, the analyzer magnet/Compton polarimeter unit will be moved back on their support table (see section 3). Then, the fiber profiler will be inserted in the beam to assess its profile and position.

Faraday Cup

*** Joe add text ***

3.3.5 Region 4 - Compton Transmission Polarimeter

The measurement of positron polarization is made by first transferring the polarization to photons using a reconversion target, and then using a photon-transmission polarimeter. The layout of the positron polarimeter is shown in Fig. 16. It is part of the experimental equipment that has been loaned to us from the SLAC E166 experiment [Ale09]. The photons that emerge from the re-conversion target (0.5 rad. len. of tungsten) are incident on an 7.5 cm long, 5 cm diameter magnetized iron absorber. Photons are transmitted through the absorber are detected in a 9-detector array of CsI (Tl) crystals that have a measured energy resolution between 3 and 4% for 0.662 MeV photons. Each

crystal is 28 cm long and 6 cm on a side.

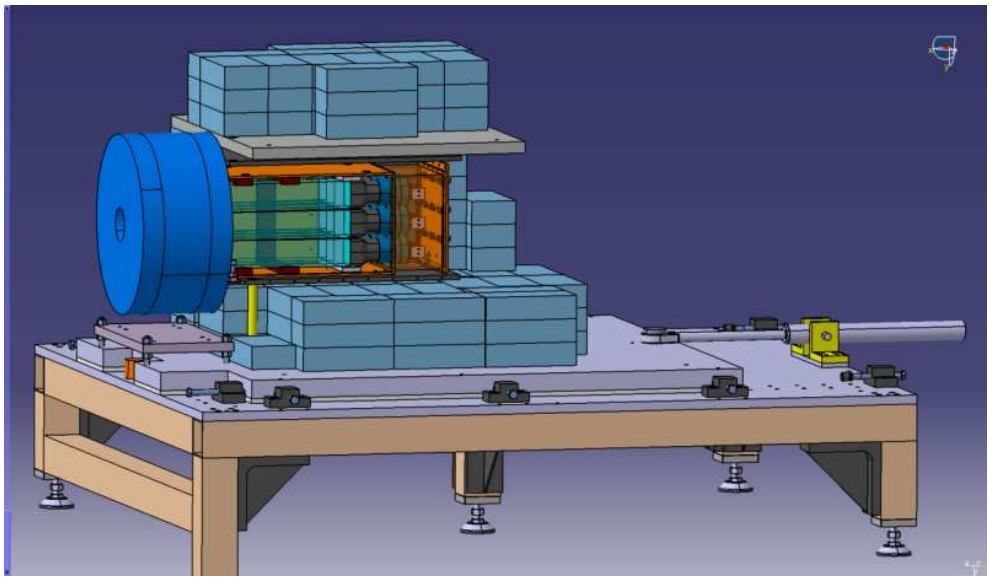

Figure 16. PEPPO positron polarimeter setup

**********comment - this section is confusing - what is the difference between the saturation procedure/polarization and the experiment? I've made some guesses but they should be checked*****

At saturation, the overall longitudinal polarization of the iron target can be calculated to be 8.19%. Saturation over most of the cylindrical core is obtained using a solenoid magnet (see Fig. 17). The average polarization of the iron target for this case is calculated to be 0.069±0.002 [Ale09]. A similar procedure will be followed to extract averaged iron polarization at the operating fields used in the experiment. The magnetic field of the iron will be measured with several pickup coils surrounding the core of the magnet. The induced-voltage signal due to a change of the magnetic flux through the pickup coil will be measured with a Precision Digital Integrator (PDI) upon field reversal. The external field map will also be measured to determine the fringe field and to constraint the Opera-3D calculation. The expected polarization error is expected to be of the same order of magnitude as that obtained for E166, ∼1%.

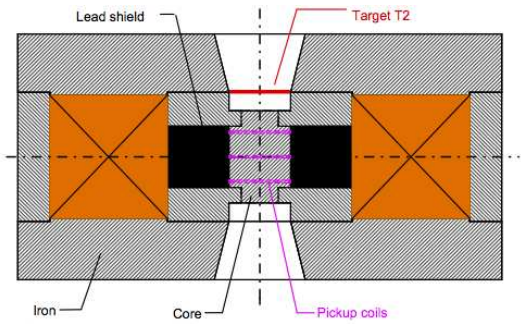

Figure 17. E166 positron analyzer magnet

Photons transmitted by the iron target will be detected in one of the nine CsI(Tl) crystals, which measure its total energy. The 9 crystals are arranged in a 3x3 array, and are stacked in a brass chamber with 6 mm wall thickness and a 2 mm thick entrance window. The box is light tight and a continuous small flow of nitrogen will evacuate the humidity and the heat. Each crystal is wrapped with two layers of white Tyvek paper to increase the scintillation light collection and with a 30μm thick copper foil to prevent cross-talk. The energy resolution of the crystals has been measured using a Cs^{137} source, which emits 0.662 MeV photons.

Each crystal is coupled to a Hamamatsu R6236 photomultiplier via a 3 mm thick sheet of optical silicon rubber. The R6236 is an 8-dynode, square photomultiplier. Its mechanical size is 6 cm $\times$ 6 cm, equivalent to the crystal size, and its photocathode is 5.4 cm $\times$ 5.4 cm. The PMTs are read out using a home-made socket that includes an amplifier ($\times 10^8$). Typical high voltage values range from 1050 V to 1400 V depending on the individual PMT's performance (the maximum for these PMTs is 1500 V). For photon energies ranging from 0.1 MeV to 5 MeV the output signal (into 50 Ohms) ranges from 40 mV to 1.9 V, suitable for the fast ADC (FADC) input.

A set of 5 scintillator paddles will be used to trigger on cosmic muons passing through the calorimeter. A coincidence of 2 scintillators above and 3 scintillators below the calorimeter will allow us to measure the minimum ionizing cosmic rays and will simultaneously provide an absolute calibration of the 9 crystals. The energy loss of a minimum ionizing muon is 40 MeV for one of our crystals. For the calibration the amplifier of the socket must be turned off; this can be done from upstairs by simply powering off the $\pm$12 V supply to the amplifier. In this case the output amplitude of the cosmic ray event will be around 140 mV and will go to a leading edge discriminator. The cosmic ray event trigger will be realized using a CAEN V895 discriminator and majority logic, which will be fired by 2 paddles out of 5. The output of the discriminator will then be sent to a TDC for offline selection. A rate of 1Hz was obtained during a test of this mode, so several hours of counting will be necessary. This calibration configuration can be used without going into the tunnel at any time when there is no beam .

A set of optical fibers coupled to the crystals will allow us to monitor the relative change in gain during operation for offline correction and time to time high voltage correction. The 1 Hz or less LED trigger is realized by using a pulser and rate divider. The LED is fired by a negative pulse with an amplitude adjusted between 0 and -3 V.

Figure 16 shows a drawing of the existing calorimeter and table of the positron polarimeter. The calorimeter is spaced by 0.5 cm from the analyzer magnet, the brass box will be surrounded by some lead blocks to minimize the background and to stop particles not coming from the analyzer target. The supporting plate of the magnet, the polarimeter and the shielding, can be moved 20 cm forward to insert some beam diagnostics such as the scintillating fiber array discussed above.

4 PEPPo modeling

A complete and full realistic description of the entire PEPPo experimental apparatus (G4PEPPo) has been developed using the Geant4 Monte Carlo simulation toolkit [Ago03,All06] version 9.4. This simulation tool is based on the SLACE166 simulation tool [Ale09] and was further extended to be more adapted to the PEPPo experiment [Dum11]. To specifically address the beam optics of the magnetic system, two codes were used: G4Beamline [Muo11] and Elegant [Ele11]. The results of this study are discussed in section **XXX**.

4.1 G4PEPPo geometries

Need a short description on how the geometry is handled ...

4.2 G4PEPPo physics

The PEPPo experiment will use incident beam energies of up to about 7 MeV. Consequently, only electromagnetic interactions are included in the simulation. The various physics processes implemented are listed in Table 2 using the four available physics packages for this energy window: the *Standard* electromagnetic package (which does not handle polarization and extends down to 100 eV), the low-energy *Livermore* package (which can handle polarization and extends down to 8 eV), the *Polarisation* package (to specifically handle polarized interactions) and the *Optical* package (to specifically handle transport of optical photons).

The choice of having more than one package for a given process has a dual purpose: (1) it provides a mean to (possibly) identify which package is more suitable for the PEPPo experiment and (2) there is seldom data for polarization transfer to benchmark simulation codes.

Need to discuss the physics options in more details ...

4.3 G4PEPPo physics

Need description of spin precession and viewing of the field maps. Also discuss G4Beamline and points to optics studies section (see with Serkan).

4.4 Background studies

Need description of the background studies ...

Table 2
The electromagnetic physics processes used in G4PEPPo. S = Standard electromagnetic package. L = Livermore low energy electromagnetic package. P = Polarization package. O = Optical package.

Particle	**Physics Process**	**Includes Polarization**	**Optional Physics**
Gammas	Photo-electric	yes	S/L/P
	Compton scattering	yes	S/L/P
	Pair production	yes	S/L/P
Electrons	Multiple (Coulomb) scattering	yes	S/L/P
	Ionisation (includes δ-rays production)	yes	S/L/P
	Bremsstrahlung	yes	S/L/P
	Möller scattering	yes	S/L/P
Positrons	Multiple (Babbah) scattering	yes	S/L/P
	Ionisation (includes δ-rays production)	yes	S/L/P
	Bremsstrahlung	yes	S/L/P
	Annihilation	yes	S/L/P
	Möller scattering	yes	S/L/P
Optical Potons	Scintillation	-	O
	Absorption	-	O
	Čerenkov radiation	-	O
	Rayleigh scattering	yes	O/L

4.5 Compton polarimeter asymmetry

Assessment of the true and false asymmetries at the Compton polarimeter ...

5 PEPPo operation

5.1 Measurement principle

The differential cross section for the Compton scattering of circularly polarized photons (P_γ) off a polarized electron target (P_t) can be written

$$\frac{d^2\sigma}{d\theta d\phi} = \frac{d^2\sigma^0}{d\theta d\phi}\left[1 + P_\gamma P_t A_C(\theta)\right] \tag{17}$$

where $d^2\sigma^0/d\theta d\phi$ is the unpolarized Compton cross section

$$\frac{d^2\sigma^0}{d\theta d\phi} = \frac{1}{2}\left(r_0\,\frac{\omega}{\omega_0}\right)^2\left[\frac{\omega_0}{\omega} + \frac{\omega}{\omega_0} - \sin^2(\theta)\right]\,\sin(\theta)\,, \tag{18}$$

and

$$A_C(\theta) = \left[\frac{\omega_0}{\omega} - \frac{\omega}{\omega_0}\right]\cos(\theta) \Big/ \left[\frac{\omega_0}{\omega} + \frac{\omega}{\omega_0} - \sin^2(\theta)\right] \tag{19}$$

is the analyzing power of the Compton process, both quantities depending on the scattered photon energy (ω) and angle (θ), and the incoming photon energy (ω_0).

Compton transmission polarimetry takes advantage of the sensivity of the Compton process to the absorption of circularly polarized photons in a polarized target. This method, which involves a single detection device matching the size of the incoming beam, is intrinsically easy to implement and has been recently used successfully in experiments similar to the present one [Fuk03,Ale09]. Considering the simple case of a monochromatic parallel photon beam scattering off a polarized electron target with length L, the transmission efficiency characterizing the probability that a photon exits the target may be written

$$\varepsilon_T = \exp\left[-(\mu_0 + P_\gamma P_t \mu_1)L\right] \tag{20}$$

which assumes the loss of any photon interacting in the target and the dominance of the Compton process; μ_0 and μ_1 are the unpolarized and polarized Compton absorption coefficients

$$\mu_0 = \rho_e \int d\theta d\phi \, \frac{d^2\sigma^0}{d\theta d\phi} \qquad \mu_1 = \rho_e \int d\theta d\phi \, \frac{d^2\sigma^0}{d\theta d\phi} A_C(\theta) \tag{21}$$

with ρ_e the electron density of the target.

The measurement of the circular polarization of the photon beam is obtained from the number of transmitted photons for opposite polarized target orientations. The corresponding asymmetry writes

$$A_T = \frac{N^+ - N^-}{N^+ + N^-} = \tanh(-P_\gamma P_t \mu_1 L) \tag{22}$$

from which the photon circular polarization is inferred according to

$$P_\gamma = -A_T / P_t \mu_1 L \,. \tag{23}$$

The associated statistical uncertainty writes

$$\delta P_\gamma = \left[2 N_\gamma \, P_t^2 \, \mu_1^2 L^2 \exp\left(-\mu_0 L\right)\right]^{-1/2} \tag{24}$$

in the case of small asymmetries.

The photon beam of this experiment constitutes of the bremsstrahlung spectrum of mono-energetic polarized electrons or positrons which energy distribution favors small photon energies while the circular polarization distribution favors high photon energies. The resulting experimental asymmetry is then a convolution of this spectrum with the polarized Compton absorption process. This multistep process has been simulated with GEANT4 [Ago03] taking

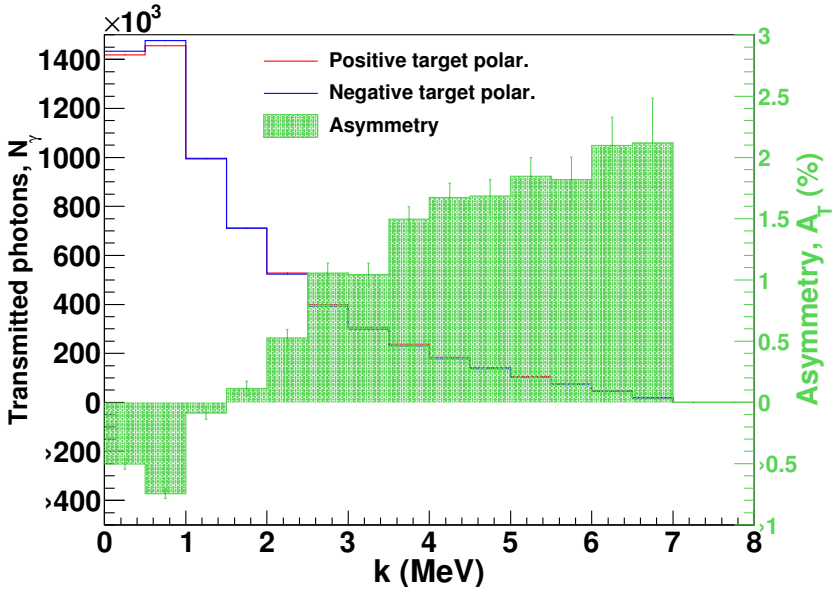

Figure 18. Number of transmitted photons for two opposite target polarization and expected experimental asymmetry as obtained from GEANT4 simulations. The statistical error bars correspond to a data taking time of 1 s at a 1 pA current.

advantage of its upgrade for polarized electron, positron and photon interactions [Dol06]. A 7.5 MeV gaussian electron beam of 400 μm width is converting into photons within a 1 mm thick tungsten target located 12 mm from a polarized target made-out from an iron cylinder 75 mm in length and 50 mm in diameter. The photon detector is symbolized by a 60×60 mm^2 ideal surface detection located 72.5 mm from the exit of the polarized target. This geometrical arrangement actually corresponds to the E166 experiment [Ale09]. Fig. 18 shows the number of transmitted photons and the expected asymmetry for 1 pA of electrons and 85 % longitudinal polarization. For each photon energy bin, the electron beam polarization can be inferred from

$$P_e = \frac{A_T}{P_t A_e} \tag{25}$$

where A_e is the electron analyzing power, determined either from simulation or experiment with a known polarized beam. The statistical average over the accepted photon energy range yields the average analyzing power $\overline{A_e} = (***valueorexpressionmissing***)$. The statistical uncertainty on P_e for a 1 s data taking time at 1 pA is $\delta P_e = (***valueorexpressionmissing***)$ meaning that an accurate measurement could be obtained within a short amount of time, provided that the detection system is able to handle a MHz event rate. Clearly, the main limitation of the statistical performance of the experiment would originate from the data acquisition rate and not the basic properties of the polarimeter.

5.2 Data acquisition

In order to achieve the statistical accuracy in a reasonable time, a fast acquisition will be designed for the readout of the CsI calorimeter. By using an aggressive pipelining and buffering of the data with the use of flash ADC one could reach easily rates of several hundreds of kilohertz of trigger rates. The proposed system is similar the current Hall A Compton polarimeter, which allowed to record up to 100KHz of trigger in 1999 [**?**]

5.3 Presentation of the device

We borrowed the transmisson Compton polarimeter hardware of SLAC experiment E166 [Ale09]. It uses a conversion target to convert most of the polarized positrons into polarized photons. The photons are then scattered from an iron target which is polarized by a magnet and detected in a segmented calorimeter. The calorimeter consists of nine CsI(Tl) blocks, each 6 cm $\times$ 6 cm $\times$ 30 cm, which were fitted with Hamamatsu PMTs. By measuring the photon asymmetry in this detector array, one can determine the initial positron's polarization.

5.4 Data acquisition system

The data acquisition system is based on the JLAB Flash ADC. This is a VME64X board with a sampling rate of 250 MHz. Having access to all the samples allows to access the polarization using different methods which could give a better control of the systematic error. The most straightforward way to measure the Compton asymmetry is to use an integrating approach. The electron beam helicity is flipped at 960 Hz, and the signal is integrated during each helicity window. The integral is the asymmetry integrated over the full range of energies of the detected photons. Since the amplitude information is available, a semi integrated method will be implemented on the VME CPU, where an histogram will be filled with the pulse energies for pulses over a certain threshold. The histograms are transferred and reset for each helicity period.

5.5 Calibration

Initial energy calibration of the calorimeter will be done using several gamma sources such as Cs^{137}, Na^{22} and Co^{60} and with cosmics. The final calibration will be done using electrons. Since it is possible to direct the electron beam to either the Mott polarimeter or the Compton transmission polarimeter, the incident beam polarization will be known at least at the 3% level. This will allow us to tune the beam through the different elements of the experiment at higher current where the beam diagnostics are fully working and to determine

the response function of the detector so that we can accurately extract the positron polarization.

5.6 Background

The unpolarized background will be eliminated in the asymmetry but will still dilute the signal. In order to reduce the polarized background, which could generate a parasitic asymmetry, large amounts of shielding will be placed around the detector. Its placement will be optimized using the Geant4 simulation. Data with the converter foil out allows us to determine the background induced by the primary electron beam. Data with the analyzer magnetic field off in the spectrometer dipoles will determine the polarized background not coming from the reconversion foil of the polarimeter.

5.7 Statistical uncertainties

By the nature of the process the efficiency of the device is quite low. Only part of the electron or positron convert into photons in the converter foil and only part of the photons will interact via Compton effect ending with Compton photons in the Cesium Iodide calorimeter

5.7.1 Integrated measure systematic uncertainties

Assuming the usual 85% electron polarization, the expected asymmetry is of the order of 1%. The pedestal width of the electronics is . So a measurement at 0.1% level, given the measured noise σ the measurement should be reached in

5.7.2 Semi-Integrated measure systematic uncertainties

The estimated positron current produced reaching the conversion target will be 1 pA for 1 uA of incident electron beam. From the Geant4 simulation of the Compton polarimeter for 5 MeV incident positron about 2.5×10^{-5} of the photons are collected in the central crystal for the highest energy bin. With this efficiency, $\sim$1% statistical accuracy is reached in about 40 seconds. The total rate of photons in the detector is estimated to be $\sim$80 kHz for 1 pA, so dead time will not be an issue even for the semi-integrated method.

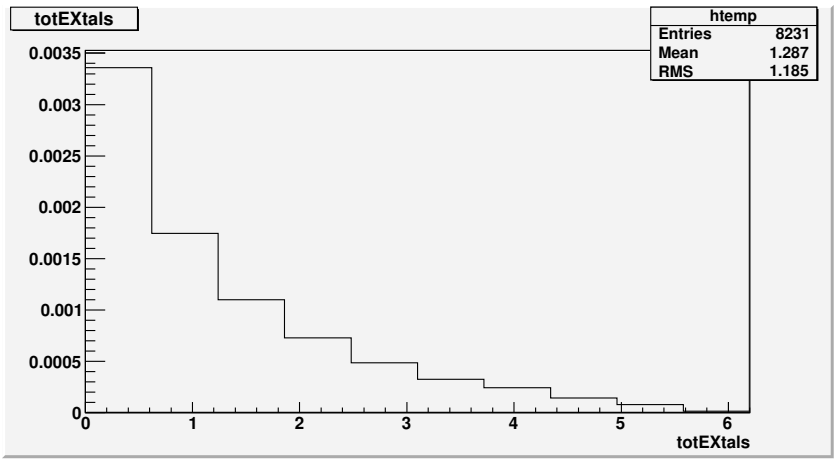

Figure 19. Number of transmitted photons for 10 energy bins and 1 million incident positrons

5.8 Polarization extraction

5.8.1 Charge asymmetry

Since we are measuring a beam asymmetry between two helicity, the charge asymmetry. In order to reduce the correction from the charge asymmetry a charge feedback acting on the source is used. Typically a charge asymmetry feedback can keep the charge asymmetry to less than 100 ppm.

5.8.2 Electronic pick-up

In a first step we will mostly run in time helicity since it makes analysis easy but makes the data potentially sensitive to pick off of helicity correlated electronic noise. In order to alleviate this problem we will still have the possibilty to run with delayed helicity. This method is common for parity experiments measure very small asymmetries. The helicity follows

5.9 Systematical uncertainties

In order to reduce the systematic, analysis will be based on pair analysis similar to the previously ran parity experiments. The fast helicity flip should allow to elimininate all false asymmetries due to slow drift such has magnets field or position changes and calibration variations.

5.9.1 Integrated measure systematic uncertainties

The integrated measurement major advantage is insensitivity to energy calibration and is free of dead time. Though the method has two systematic on the extraction of the polarization :

- the detector non-linearities
- contribution of polarized background.
- dilution by background

Detector linearity will be checked using a pulser and folded in the simulation to extract the polarization. Contribution of background can be determined with the runs with analyzer field on, off and flipped.

5.9.2 Semi-integrated E166 systematic uncertainties

An semi-integrated method is interesting to be studied since the asymmetry grows with energy. Nevertheless this method is very sensitive to the energy calibration of the detector, since the shape of the asymmetry as a function of the energy is fitted to extract the polarization. The systematic uncertainty of this method are :

- PMT gain change as a function of time
- energy response of the detector
- pile up
- position in the detector which can induce leakage.

The relative gain will be monitored by a LED system and regularly checked with radioactive sources to provide an absolute calibration, Contribution of the pile up will be determined with data taking at different currents and running the DAQ in sampling mode to record the full waveforms to study the contribution of the pile up. Response function of the detector will be modeled by the simulation. The data can be cross checked at a photon source such as TUNL in Duke in needed. Collimated runs and looking at the behavior of the asymmetry when more than one block is hit will be taken to assess the effect of leakage to the neighboring blocks.

6 Beam time request

6.1 Commissioning

6.2 Electron calibration

6.3 Positron measurements

6.4 Beam requirements

We request approval for 336 hours (2 weeks) of beam time to measure the polarization of positrons produced in the JLab injector. The commissioning of a new beam line and the Compton transmission polarimeter is estimated to

take 112 hours of beam time with the remaining 224 hours devoted to beam polarization,, current, and spot size measurements. Emittance measurements will consume about 24 hours of the commissioning time. The commissioning of new beam line monitors and establishing the beam transport to the Compton transmission polarimeter with consume 88 hours.

Running Condition Number	Beam Energy (MeV)	Beam Current (μA)	Beam Polarization (%)	Target Material	Target Thickness (mg/cm^2)	Beam Time (h)
1	6.2	1-5	> 80	Mott Targ.		10
2	6.2	1-10	> 80	W Con. #1	192.5	142
				W Con. #2	1925	
				W Con. #3	3850	
				Pol. Conv. #1	1925	
				Pol. Conv. #2	3369	
				Pol. Targ.	59055	
3	6.2	1-10	> 80	Ann. Targ.	1925	72
				Fiber Detector		

Table 3

Beam polarization measurements made with the Mott and Compton transmission polarimeters will take more than half of the allotted 224 hours. The first measurement will compare the polarization of a 6.2 MeV electron beam measured using the Mott polarimeter to the polarization measured in the Compton transmission polarimeter. A Tungsten converter target will be inserted to produce positrons. We plan to repeat the electron polarization measurement with the Tungsten target inserted using the Compton transmission polarimeter for comparison and then proceed with a positron polarization measurement. Positron polarization measurements will be done for four addition positron energies; 1, 2, 3, and 4 MeV. As shown in Figure reffg:as, the measured photon transmission asymmetry in the Compton transmission polarimeter changes sign when going from 1 to 3 MeV. The transmitted photon rate is predicted to be a factor of 3 higher at 1 MeV than at 2 MeV while the asymmetries are equivalent in magnitude (0.5%) but opposite in sign. The largest asymmetry of 2 % is predicted to occur at 6 MeV for the range of energies we are probing. Table **??** identifies the beam time for the physics measurements performed by this experiment.

Appendicies

Appendix I: Polarization transfer in the bremsstrahlung and pair production processes

In this appendix we review the theoretical descriptions available for polarization transfer in the bremsstrahlung and pair production processes relevant for the proposed polarized positron source. The present proposal will not study these with the detail necessary to do more than demonstrate the feasibility of using these processes (in conjunction with an intense beam of highly polarized electrons) to produce polarized positrons. However, the experiment will develop and commission an apparatus that will support further relevant measurements in follow-on experiments.

A relativistic approach to the description of the bremsstrahlung process

As the essential mechanism for the production of high energy photons, the bremsstrahlung process is a text-book reaction widely investigated theoretically and experimentally. Polarization observables were first addressed by H. Olsen and L. Maximon [Ols59] (hereafter referred to as OM) within the Born approximation for relativistic and small angle particles, including effects of the nuclear field screening and corrections to the Born approximation. These are still the reference calculations implemented in the GEANT4 simulation package [Ago03,Dol06]. The circular polarization transfer is essentially universal, the highest circular polarization being obtained at the highest photon energy (Fig. 20 left). A similar behaviour is observed at low energies but with the additionnal feature of an unphysical region close to the end point of the spectra (Fig. 20 right). This appears in the calculations as a consequence of the well-known tip problem: due to too large Coulomb corrections for heavy nuclei, the OM unpolarized differential cross section passes through zero and becomes negative. This translates into a singularity for the polarization transfer in the tip region.

As a reciprocal process of the bremsstrahlung reaction, pair production is described by the same matrix elements so that the relations for experimental observables can be derived from the bremsstralhung expressions following elementary substitutions [Ols59]. The polarization transfer from circular photons to longitudinal positrons appears to be more sensitivite to the initial photon energy than in the bremsstrahlung case. These calculations clearly show some singular behaviour even at high energy (Fig. 21 left) i.e. in a region where OM approximations are expected to be valid. It is even more stricking at low energy where these relations yield unphysical results (Fig. 21 right) over a large part if not all of the kinematic phase space. As surprising as it may be, polarization phenomena in the pair creation process are not understood within OM prescription.

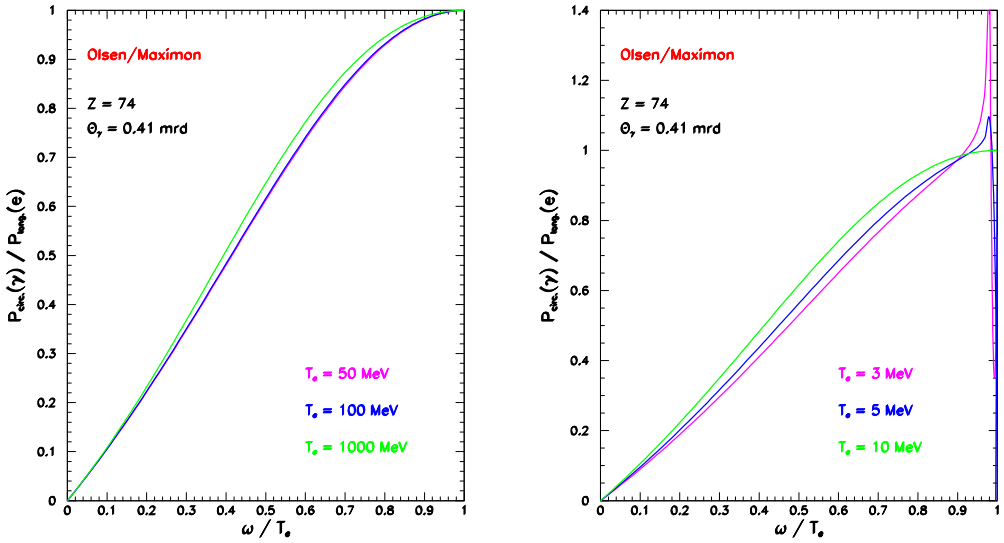

Figure 20. Longitudinal to circular polarization transfer for the bremsstrahlung process according to OM prescription at high (left) and low (right) initial electron kinetic energy.

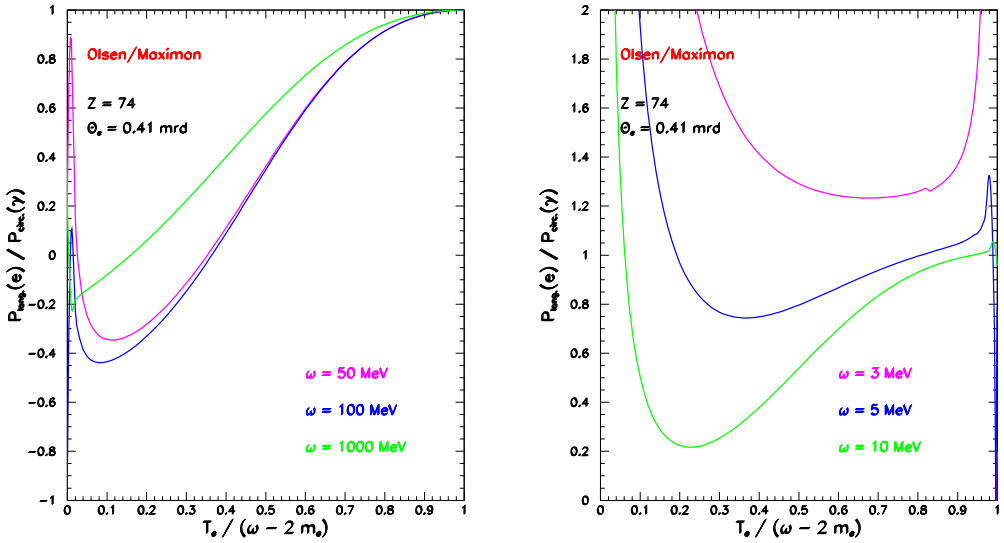

Figure 21. Circular to longitudinal polarization transfer for the pair creation process according to OM prescription at high (left) and low (right) initial photon energy.

Electron mass effects in bremsstrahlung and pair production

These phenomena were recently revisited by E. Kuraev *et al.* [Kur10] (hereafter referred to as KBST) taking advantage of modern techniques to reformulate in the infinite momentum frame the matrix elements of the bremmstrahlung and pair creation reactions. Polarization observables are re-derived within this framework in the Born approximation, neglecting Coulomb corrections but considering screening effects and specifically taking into account the effects of finite electron mass.

The KBST calculations don't exhibit any of the singular features of OM cal-

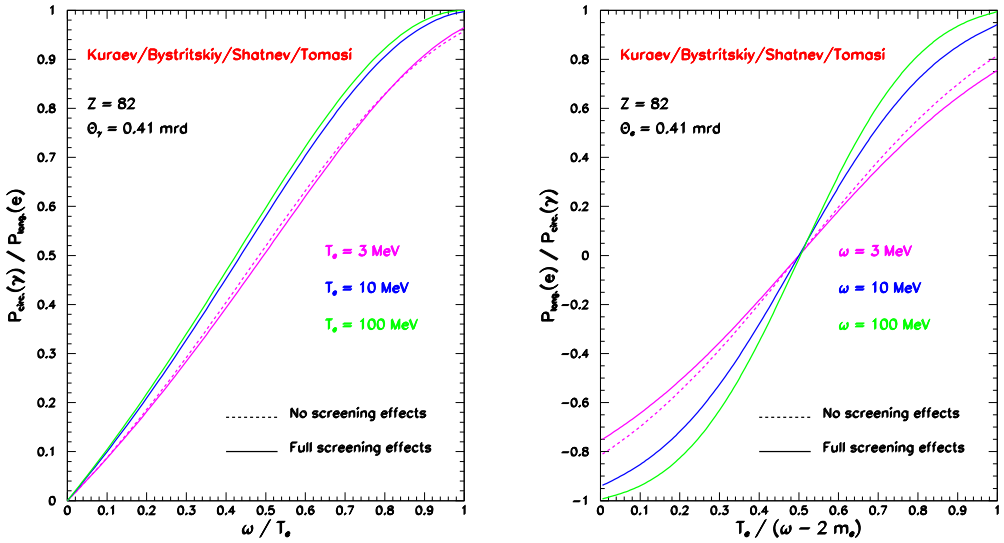

Figure 22. Longitudinal polarization transfer in the bremsstrahlung process (left) and circular polarization transfer in the pair creation process according to the KBST prescription at different initial energies.

culations and the comparison between the two extreme screening situations (none and full) show moderate and controlled effects (Fig. 22). The description of the bremsstrahlung process is numerically very close to OM and is free of end-point effects. Furthermore, within the KBST approach, the polarization transfer for the pair creation process possesses the very remarkable feature of a kinematical symmetry. It is indeed quite natural to expect such a symmetry in a process where only two particles with same mass and spin are produced. The differences between OM and KBST calculations for this process (Fig. 23) are the largest at small energy and persist significantly at high energy as a consequence of the observed kinematical symmetry.

The main result of this new approach is a consistent description of both the bremmsstrahlung and pair creation processes with no constraint on the initial beam energy. This is a direct consequence of the finitie mass of the electron and is further supported by noticing that OM calculations become unphysical in kinematical regions where the electron mass is important: when the initial electron gives all of its kinetic energy to the photon (bremmstrahlung); when one particle of the e^+e^- pair is produced at rest; and also at low photon energy (pair creation). Even if bremsstrahlung and pair creation are reciprocal processes, some of the OM approximations valid for the bremsstrahlung reaction cannot be exported to the pair creation process.

By measuring the polarization transfer from longitudinal electrons to longitudinal positrons at low energy using a thin target, the PEPPo experiment will demonstrate the basic processes we intend to use to develop a next generation polarized positron source. The apparatus developed will permit a followon experiment to provide the data necessaryto understand polarization phenomena in the pair creation process in detail. We would expect that it will verify the accuracy of the KBST description as an improvement on the OM description. Once this has been demonstrated, we would endeavor to enhance GEANT

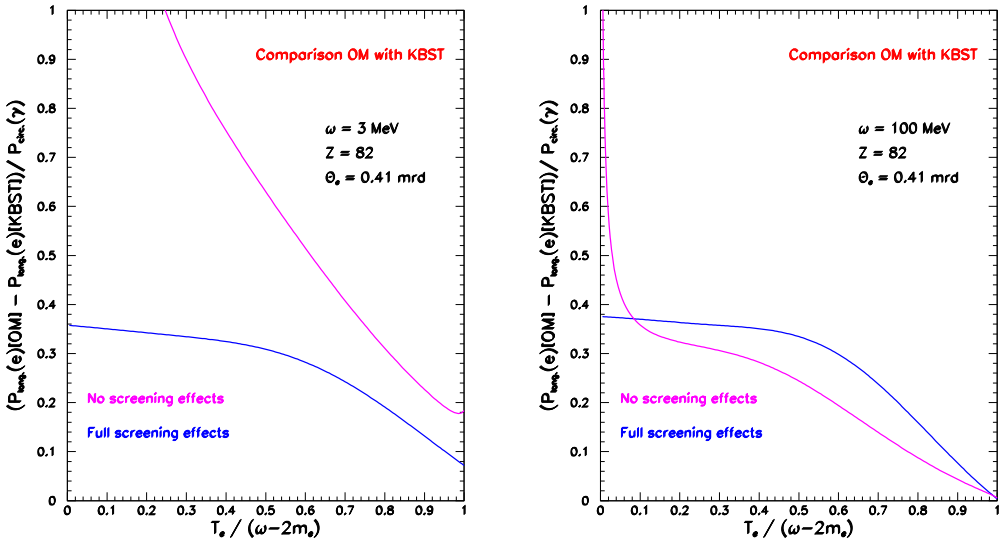

Figure 23. Difference between OM and KBST prescriptions for the circular polarization transfer in the pair creation process at low (left) and high (right) initial photon energy.

to incorporate KBST theory, and then use the enhanced code to carry out numerical simulations that would permit us to optimze the design of a new polarized positron source.

Appendix II: Two photon effects in the determination of the nucleon's electromagnetic form factors from elastic electron scattering data

In this appendix we review the theoretical understanding of two photon effects in the determination of the nucleon's electromgnetic form factors from elastic electron scattering data and the potential utility of an intense beam of polarized positrons to refine the experimental verification of theoretical efforts to incorporate these effects. The present proposal will not study two photon effects, but will be a step toward the determination of the feasibility of future experiments that would focus on such measurements.

Nucleon electromagnetic form factors

The elastic scattering of an electron beam off a proton target is an elementary process for the study of the internal structure of the proton. In the reaction $e(k) + P(p) \rightarrow e(k') + P(p')$, symbolized on Fig. 24, the squared four-momentum transfer of the virtual photon $q^2 = (k - k')^2 = (p' - p)^2$ characterizes the transverse size of the probed internal region of the proton which electromagnetic structure is described by the electric (G_E) and magnetic (G_M) form factors. The electromagnetic form factors are consequently depending only on q^2. Within a non-relativistic approach, these quantities can be interpreted as the Fourier transforms of the charge and magnetization densities of the proton [Kel02].

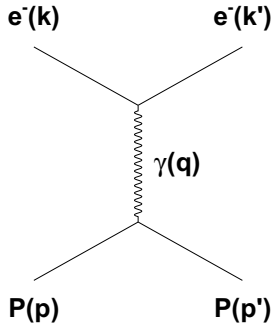

Figure 24. lowest order (QED) diagram of the elastic eP reaction; the initial and final electron mometum four-vectors are k and k', respectively, and p and p' for the proton; the four-momentum transfer to the photon is q.

In the Born approximation, that is the one photon exchange approximation, the scattering amplitude $\mathcal{M}$ is defined by the interaction of the electromagnetic ($J^{\nu,e}$) and hadronic ($J^{\mu,P}$) currents as

$$\mathcal{M} = \underbrace{\overline{u}(k')e\gamma^{\mu}u(k)}_{J^{\nu,e}} \frac{eg_{\mu\nu}}{q^2} \underbrace{\overline{u}(p')\left[G_M\gamma^{\mu} + \frac{G_E - G_M}{2M(1+\tau)}(p+p')^{\mu}\right]u(p)}_{J^{\mu,P}}$$

where u is the electron spinor, $2g^{\mu\nu} = \{\gamma^{\mu}, \gamma^{\nu}\}$ is the Minkowski metric tensor, M is the proton mass, and $\tau = -q^2/4M^2$. The proton electromagnetic form

factors can be experimentally measured from different observables that are derived from the scattering amplitude.

Experimental observables

The electromagnetic form factors G_M and G_E can be obtained from unpolarized and polarized experimental observables.

For unpolarized beam and target, the form factors are extracted from the unpolarized cross section following a so-called Rosenbluth separation. The cross section for the unpolarized elastic process, first derived by M.N. Rosenbluth [Ros50], is function of the four-momentum transfer and the electron scattering angle (θ_e)

$$\frac{d\sigma}{d\Omega_e} = k f_{rec} \left(\frac{d\sigma}{d\Omega_e}\right)_{Mott} \sigma_R = k f_{rec} \left(\frac{d\sigma}{d\Omega_e}\right)_{Mott} \left[G_M^2 + \frac{\epsilon}{\tau} G_E^2\right]$$

where $k = 1/\left[\epsilon\tau(1+\tau)\right]$ is a kinematical factor, $f_{rec} = E'/E$ is the recoil correction factor, and

$$\epsilon = \left[1 + 2(1+\tau)\tan^2(\theta_e/2)\right]^{-1}$$

is the longitudinal polarization degree of the virtual photon. The Mott cross section represents the elastic electron scattering off a point-like particle, and the reduced cross section σ_R is the quantity of interest which contains the internal structure of the nucleon. The form factors are separated taking advantage of the ϵ-dependence of σ_R: the magnetic form fator is measured at large scattering angles ($\theta_e \sim 180°$) where G_M dominates σ_R, and the electric form factor is extracted from a measurement at small scattering angles ($\theta_e \sim 0°$) keeping τ (i.e. q^2) constant by changing the beam energy.

The polarization transfer from the electron beam to the recoil proton in the reaction $\vec{e}p \to e\vec{p}$ offers an alternative determination of the electric form factor [Akh74,Arn81]. In this process, the perpendicular (P_t) and longitudinal (P_l) polarization of the recoil proton write

$$P_t = -\frac{P_b}{\sigma_R}\sqrt{\frac{2\epsilon(1-\epsilon)}{\tau}}\, G_E G_M$$
$$P_l = \frac{P_b}{\sigma_R}\sqrt{1-\epsilon^2}\, G_M^2$$

where P_b is the electron beam polarization. The ratio of the polarization component yields a unique determination of the form factors ratio

$$\frac{G_E}{G_M} = -\sqrt{\frac{\tau(1+\epsilon)}{2\epsilon}}\,\frac{P_t}{P_l}$$

which, combined with the simultaneous measurement of the reduced cross section, allows for a new separation of the electromagnetic form factors.

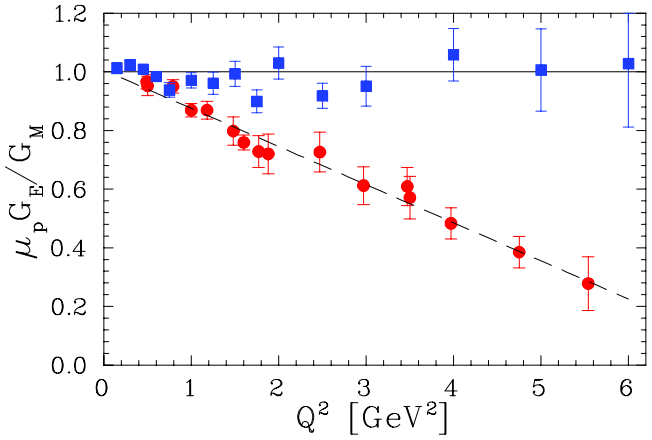

Figure 25. most recent experimental data on the electromagnetic form factor ratio as measured from polarization transfer [Jon00,Gay02,Puc10] and Rosenbluth separation [And94,Chr04,Qat05] experiments.

This ratio has been extensively studied using the methods described previously (note that the Rosenbluth separation access the squared ratio and does not teach about the relative sign of the form factors, conversely to the polarization method). The most recent data are shown on Fig. 25 where a striking discrepancy between the two technics is revealed and has been confirmed over the past years. These disagreements generated a lot of controversy and it was suggested that they may originate from higher order mechanisms beyond the Born approximation. The exchange of two photons in the ep reaction was shown to possibly reconcile these two techniques [Gui03].

Indeed, the 2γ-exchange process brings corrections to the form factors and to the experimental observables. The internal structure of the proton is no longer represented by two but five form factors

$$\begin{aligned}\widetilde{G}_M &= -e_b G_M + \delta\widetilde{G}_M \\ \widetilde{G}_E &= -e_b G_E + \delta\widetilde{G}_E \\ \widetilde{F}_3 &= \delta\widetilde{F}_3\end{aligned}$$

where e_b stands for the sign of the lepton beam charge. The modified experimental observables write [Gui03]

$$\begin{aligned}\sigma_R &= G_M^2 + \frac{\epsilon}{\tau}G_E^2 - 2e_b\, G_M\, \Re\left[\delta\widetilde{G}_{M,1}\right] - 2e_b\, \frac{\epsilon}{\tau}G_E\, \Re\left[\delta\widetilde{G}_{E,1}\right] \\ P_t &= -\frac{P_b}{\sigma_R}\sqrt{\frac{2\epsilon(1-\epsilon)}{\tau}}\left(G_E G_M - e_b\, G_E \Re[\delta\widetilde{G}_M] - e_b\, G_M \Re\left[\delta\widetilde{G}_{E,1}\right]\right) \\ P_l &= \frac{P_b}{\sigma_R}\sqrt{1-\epsilon^2}\left(G_M^2 - 2e_b\, G_M \Re\left[\delta\widetilde{G}_{M,2}\right]\right)\end{aligned}$$

with

$$\delta\widetilde{G}_{M,1} = \delta\widetilde{G}_M + \epsilon\frac{\nu}{M^2}\widetilde{F}_3$$
$$\delta\widetilde{G}_{E,1} = \delta\widetilde{G}_E + \frac{\nu}{M^2}\widetilde{F}_3$$
$$\delta\widetilde{G}_{M,2} = \delta\widetilde{G}_M + \frac{\epsilon}{1+\epsilon}\,\frac{\nu}{M^2}\widetilde{F}_3$$
$$\nu = \frac{p+p'}{2}.\frac{k+k'}{2}\,.$$

The separate determination of the Born terms and of the 2γ-exchange corrections require at minima a set of five different measurements. Polarized electrons and polarized positrons provide six independent observables which allow for a complete model independent extraction of these quantities.

Appendix III: Solid state structure studies

Positron Annihilation Spectroscopy (PAS) is a well-know technique for the investigation of the structure of materials [JPos09] that would benefit from the development of a high intensity polarized positron source. PAS is used for the study of defects and vacancies in semi-conductors [Kra99]. It relies on the annihilation of very low energy positrons with atomic electrons of the material and the subsequent detection of one or both of the pair of the annihilation-generated photons. The decay time of this process is directly related to the electron density at the annihilation site. Furthermore, the motion of atomic electrons induce a Doppler broadening of the 511 keV γ-rays and a distortion of the back-to-back angular correlation. Consequently, the measurement of the energy distribution, or the angular correlation between annihilation γ-rays permits us to characterize the material via the determination of the momentum distribution of atomic electrons (Fig. 26).

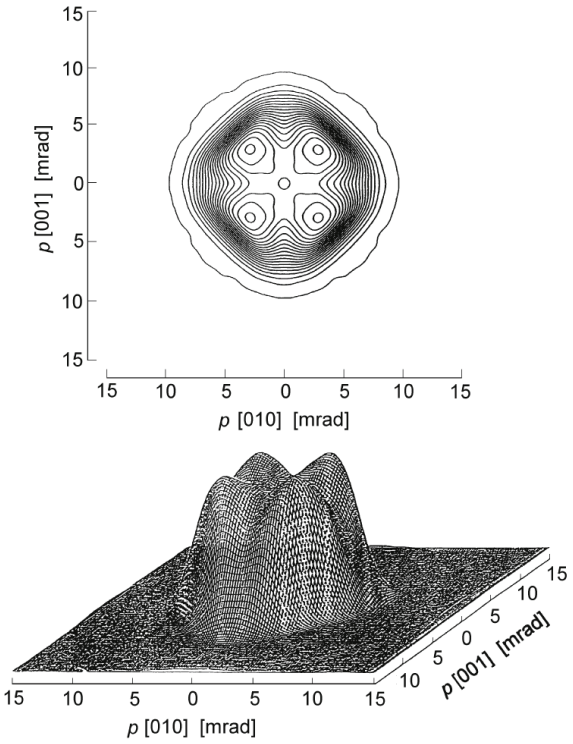

Figure 26. Two-dimensional angular correlation of annihilation radiation in gallium arsenide exhibiting no positron trapping in defects [Tan95].

However, this powerful technique, known as 2D-ACAR, is limited by the intensity of the available positron beams, which are typically obtained from radioactive sources. The generation of positrons from low energy polarized electrons is expected to deliver a positron flux that is 100 times higher [Ang10]. Together with polarization capabilities, such an accelerator based thermalized positron source would be a breakthrough for PAS studies.

References

[Ago03] S. Agostinelli *et al*, Nucl. Inst. Meth. **A 506** (2003) 250.

[Air01] A. Airapetian *et al.*, *Phys. Rev. Lett.* **87** (2001) 182001.

[Akh74] A. L. Akhiezer, M. P. Rekalo, Sov. J. Part. Nucl. **3** (1974) 277.

[Ale08] G. Alexander *et al*, Phys. Rev. Lett. **100** (2008) 210801.

[Ale09] G. Alexander *et al*, Nucl. Inst. Meth. **A 610** (2009) 451.

[All06] J. Allison *et al.*, *Geant4 developments and applications*, IEEE Transactions on Nuclear Science, **53**, p. 270-278 (2006).

[And94] L. Andivahis *et al.*, Phys. Rev. D **50** (1994) 5491.

[Ang10] V. Angelov, E. Voutier, *work in progress.*

[Arn81] R. G. Arnold, C. E. Carlson, F. Gross, Phys. Rev. C **23** (1981) 363.

[Arr03] J. Arrington, Phys. Rev., **C68**, 034325 (2003).

[Arr04] J. Arrington, Phys. Rev., **C69**, 032201 (2004).

[Arr06] J. Arrington, *et al.*, Jefferson Lab Proposal PR-07-005 (2003) unpublished.

[Arr07] J. Arrington, C. D. Roberts and J. M. Zanotti, J. Phys. G **34**, S23 (2007).

[Bel02] A.V. Belitsky, D. Müller, *Nucl. Phys.* **A 711** (2002) 118c.

[Bel05] A.V. Belitsky, A.V. Radyushkin, *Phys. Rep.* **418** (2005) 1.

[Ben95] O. Benhar, A. Fabrocini, S. Fantoni, I. Sick, Phys. Lett. **B343** (1995) 4752.

[Ber06] P.-Y. Bertin, C.E. Hyde, C. Muñoz Camacho, J. Roche *et al.*, *Jefferson Lab Prop.* **PR-07-007** 2007.

[Bes96] E. G. Bessonov, A. A. Mikhailichenko, *Proc. of the V^{th} European Particle Accelerator Conference*, Barcelona (Spain), June 10-14, 1996.

[Bur00] M. Burkardt, *Phys. Rev.* **D 62** (2000) 071503.

[Bur05] M. Burkardt, *Phys. Rev.* **D 72** (2005) 094020.

[Car07] C. E. Carlson and M. Vanderhaeghen, Ann. Rev. Nucl. Part. Sci. **57**, 171 (2007).

[Chr04] M. E. Christy *et al.*, Phys. Rev. C **70** (2004) 015206.

[Col99] J.C. Collins, A. Freund, *Phys. Rev.* **D 59** (1999) 074009.

[Die02] M. Diehl, *Eur. Phys. Jour.* **C 25** (2002) 223.

[Die03] M. Diehl, *Phys. Rep.* **388** (2003) 41.

[Die09] M. Diehl, *CLAS12 European Workshop*, Genova (Italy), February 25-28, 2009;
http://www.ge.infn.it/∼clas12/talks/thursday_session6/diehl-genova.pdf

[Dol06] R. Dollan, K. Laihem, A. Schälicke, Nucl. Inst. Meth. **A 559** (2006) 185S.

[Dum09a] J. Dumas, J. Grames, E. Voutier, *AIP Conf. Proc.* **1149** (2009) 1184.

[Dum09b] J. Dumas, J. Grames, E. Voutier, *AIP Conf. Proc.* **1160** (2009) 120.

[Dum11] J. Dumas, Ph.D. thesis, Université Joseph Fourier, Grenoble, France (2011).

[Ele11] Elegant code for electron transport, http://www.anl.gov

[Fuk03] M. Fukuda *et al*, Phys. Rev. Lett. **91** (2003) 164801.

[Gir08] F.-X. Girod, R.A. Niyazov *et al.*, *Phys. Rev. Lett.* **100** (2008)162002.

[Gay02] O. Gayou, *et al.*, Phys. Rev. Lett. **88**, 092301 (2002).

[Gue98] P. Guèye *et al.*, Phys. Rev, **C57**, 2107 (1998).

[Gue99] P. Guèye *et al.*, Phys. Rev. **C60**, 044308 (1999).

[Gra07] J. Grames *et al.*, *Proc. of the 2007 Particle Accelerator Conference*, Albuquerque (New Mexico, USA), June 25-29, 2007.

[Gui03] P. A. M. Guichon, and M. Vanderhaeghen, Phys. Rev. Lett. **91**, 142303 (2003).

[Gui08] M. Guidal, *Eur. Phys. J.* **A 37** (2008) 319.

[HallB07] Proposal E-07-005: *"Beyond the Born Approximation: A precise Comparison of e^+p and e^-p elastic Scattering in CLAS"*, A. Afanasev *et al.* (2007) http://wwww.jlab.org/Hall-B .

[Ji97] X. Ji, *Phys. Rev. Lett.* **78** (1997) 610.

[Ji98] X. Ji, J. Osborne, *Phys. Rev.* **D 58** (1998) 094018.

[Jon00] M. K. Jones, *et al.*, Phys. Rev. Lett. **84**, 1398 (2000).

[Jou96] J. Jourdan, Nucl. Phys., **A603** (1996) 117160.

[JPos09] Proceedings of the International Workshop on Positron at Jefferson Lab, Edts. L. Elouadrhiri, T.A. Forest, J. Grames, W. Melnitchouk, and E. Voutier, *AIP Conf. Proc.***1160** (2009).

[Kel02] J. J. Kelly, Phys. Rev. C **66**, 065203 (2002).

[Kur10] E. A. Kuraev, Y. M. Bystritskiy, M. Shatnev, E. Tomasi-Gustafsson, *Phys. Rev. C* **81** (2010) 055208.

[Kra99] R. Krause-Rehberg, H.S. Leipner, *Positron Annihilation in Semiconductors*, ISBN 3-540-64371-0 Springer-Verlag Berlin Heidelberg New York, 1999.

[Maa05] F. E. Maas *et al.*, *Phys. Rev. Lett.* **94** (2005) 152001.

[Maz07] M. Mazouz, A. Camsonne, C. Muñoz Camacho, C. Ferdi, G. Gavalian, E. Kuchina *et al.*, *Phys. Rev. Lett.* **99** (2007) 242501.

[McM61] W.H. McMaster, *Rev. Mod. Phys* **33** (1961) 8.

[Mec03] B.A. Mecking *et al.*, *Nucl. Inst. Meth.* **A 503** (2003) 513.

[Mez11] M. Meziane *et al.*, Phys. Rev. Lett. **106** (2011) 132501.

[Mil03] G. A. Miller, Phys. Rev. C **68**, 022201 (2003).

[Mil07] G. A. Miller, Phys. Rev. Lett. **99**, 112001 (2007).

[Mil08] G. A. Miller, and J. Arrington, Phys. Rev. **C78**, 032201 (2008).

[Mil09] G. A. Miller, and J. Arrington (2009), arXiv:0903.1617.

[Moh08] P. J. Mohr, B. N. Taylor, and D. B. Newell, Rev. Mod. Phys. **80**, 633 (2008).

[Mot09] M. Moteabbed, Ph.D. thesis, *A Precise Measurement of the Two-Photon Exchange effect*, Florida International University (2009).

[Mou09] H. Moutarde, *Phys. Rev.* **D 74** (2009) 094021.

[Mul94] D. Müller, D. Robaschick, B. Geyer, F.M. Dittes, J. Hořejši, *Fortschr. Phys.* **42** (1994) 101.

[Mun06] C. Muñoz Camacho, A. Camsonne, M. Mazouz, C. Ferdi, G. Gavalian, E. Kuchina *et al.*, *Phys. Rev. Lett.* **97** (2006) 262002.

[Muo11] Muons Inc., *The G4Beamline software*, http://www.muonsinc.com

[Ols59] H.A. Olsen, L.C. Maximon, *Phys. Rev.* **114** (1959) 887.

[OLY08] Proposal PRC-20080909, R. Milner *et al.* (2008) unpublished.

[Omo06] T. Omori *et al*, Phys. Rev. Lett. **96** (2006) 114801.

[Per07] C. F. Perdrisat, V. Punjabi, and M. Vanderhaeghen, Prog. Part. Nucl. Phys. **59**, 694764 (2007).

[Pho10] R. Pohl, *et al.*, Nature **466**, 213 (2010).

[Pot97] A.P. Potylitsin, *Nucl. Inst. Meth.* **A 398** (1997) 395.

[Puc10] A. J. R. Puckett *et al.*, Phys. Rev. Lett. **104** (2010) 242301.

[Puc11] A. J. R. Puckett *et al.*, arXiv:1102.5737v2 (submitted to Phys. Rev. C).

[Qat05] I. A. Qattan, *et al.*, Phys. Rev. Lett. **94**, 142301 (2005).

[Rad97] A.V. Radyushkin, *Phys. Rev.* **D 56** (1997) 5524.

[Ral02] J.P. Ralston, B. Pire, *Phys. Rev.* **D 66** (2002) 111501.

[Ros50] M. N. Rosenbluth, Phys. Rev. **79**, 615 (1950).

[Ros00] R. Rosenfelder, Phys. Lett. **B479**, 381 (2000).

[Sai11] Saint-Gobain Crystals, http://www.detectors.saint-gobain.com.

[Sic03] I. Sick, Phys. Lett.. **B576**, 62 (2003).

[Sok64] A. A. Sokolov and I. M. Ternov (1964) Sov. Phys. Dokl. **8** (1964) 1203.

[Sol09] P. Solvigon, D. Gaskell and J. Arrington (2009), arXiv:0906.0512.

[Ste01] S. Stepanyan *et al.*, *Phys. Rev. Lett.* **87** (2001) 182002.

[Tan95] S. Tanigawa, A. Uedono, L. Wei, R. Suzuki, *Positron Spectroscopy of Solids*, A. Dupasquier, J. Mills eds., IOS Press Amsterdam, 1995, 729.

[Whi74] R.R. Whitney *et al.*, Phys. Rev. **C9** (1974) 22302235.